CHEMISTRY
A EUROPEAN JOURNAL

DOI: 10.1002/chem.200800588

# Copper Complexes of Mono- and Ditopic [(Methylthio)methyl]borates: Missing Links and Linked Systems En Route to Copper Enzyme Models

**Kai Ruth, Sandor Tüllmann, Hannes Vitze, Michael Bolte, Hans-Wolfram Lerner, Max C. Holthausen,* and Matthias Wagner*[a]**

**Abstract:** TMEDA-free (TMEDA: tetramethylethylenediamine) $LiCH_2SMe$ is a suitable reagent for the selective introduction of (methylthio)methyl groups into $PhBBr_2$ and its *p*-silylated derivative $Me_3Si{-}C_6H_4{-}BBr_2$. The resulting compounds, $R^*{-}C_6H_4{-}B(Br)(CH_2SMe)$ ($R^*=H$: **2**; $R^*=SiMe_3$: **7**) and $PhB(CH_2SMe)_2$ (**3**), form cyclic dimers through B–S adduct bonds in solution and in the solid state. Compounds **2** and **3** have successfully been used for preparing the ($N_2S$) scorpionate $[PhBpz_2(CH_2SMe)]^-$ ($[\mathbf{5}]^-$) (pz: pyrazol-1-yl) and the ($NS_2$) scorpionate $[PhBpz(CH_2SMe)_2]^-$, respectively. Compound **7** proved to be an excellent building block for the heteroditopic poly(pyrazol-1-yl)borate *p*-$[pz_3B{-}C_6H_4{-}Bpz_2(CH_2SMe)]^{2-}$ ($[\mathbf{10}]^{2-}$) that mimics the two ligation sites of the copper enzymes peptidylglycine α-hydroxylating monooxygenase and dopamine β-monooxygenase. Treatment of the monotopic tripod $[\mathbf{5}]^-$ with CuCl and $CuBr_2$ results in the formation of complexes $K[Cu(\mathbf{5})_2]$ and $[Cu(\mathbf{5})_2]$. An X-ray crystallography study of $K[Cu(\mathbf{5})_2]$ revealed a tetrahedral ($N_2S_2$) coordination environment for the $Cu^I$ ion, whereas the $Cu^{II}$ ion of $[Cu(\mathbf{5})_2]$ possesses a square-pyramidal ($N_4S$) ligand sphere (S-atom in the axial position). The remarkable redox properties of $K[Cu(\mathbf{5})_2]$ and $[Cu(\mathbf{5})_2]$ have been assessed by cyclic voltammetry and quantum chemical calculations. The reaction of $K[Cu(\mathbf{5})_2]$ with dry air leads to the $Cu^{II}$ species $[Cu(\mathbf{5})_2]$ and to a tetranuclear $Cu^{II}$ complex featuring $[PhB(O)pz_2]^{2-}$ ligands. Addition of CuCl to $K_2[\mathbf{10}]$ gives the complex $K_3[Cu(\mathbf{10})_2]$ containing two ligand molecules per $Cu^I$ center. The $Cu^I$ ion binds to both heteroscorpionate moieties and thereby establishes a coordination environment similar to that of the $Cu^I$ ion in $K[Cu(\mathbf{5})_2]$.

**Keywords:** borates · copper · metalloenzymes · N,S ligands · tripodal ligands

## Introduction

For several decades now, tris(pyrazol-1-yl)borate (scorpionate) ligands **A** are widely used in bioinorganic and organometallic chemistry (Figure 1).[1,2] Part of this success is owed to the fact that introduction of appropriate substituents, $R^1$, into the 3-positions of the pyrazolyl rings allows extensive control over the steric demand of the ligands, and thus over their ability to kinetically stabilize reactive complex fragments. By contrast, an adjustment of the ligand field strengths of tris(pyrazol-1-yl)borates is much harder to achieve, because electronic substituent effects of $R^1$–$R^3$ on the donor properties of the pyrazolyl rings turned out to be rather modest.

One way to alter the donor/acceptor properties of scorpionate ligands over a wider range is to replace the pyrazolyl rings by phosphorus- (**B**[3–5]) or sulfur-containing groups (**C**,[6,7] **D**;[8–12] Figure 1). Similar to the parent scorpionates **A**, ligands **B**–**D** provide a monoanionic, tridentate, face-capping coordination mode, but they differ from **A** with regard to the softness of their donor sets. Moreover, in the thioimidazolyl derivatives **C**, the boron atom is separated from the donor atoms by three bonds as opposed to two bonds in **A**.

Very recently, even hybrid scorpionates of **A**–**D** have become available, which provide nitrogen and phosphorus

[a] Dipl.-Chem. K. Ruth, Dipl.-Chem. S. Tüllmann, Dipl.-Chem. H. Vitze, Dr. M. Bolte, Dr. H.-W. Lerner, Prof. Dr. M. C. Holthausen, Prof. Dr. M. Wagner
Institut für Anorganische und Analytische Chemie
Johann Wolfgang Goethe-Universität Frankfurt am Main
Max-von-Laue-Straße 7, 60438 Frankfurt (Germany)
Fax: (+49) 69-798-29260
E-mail: Max.Holthausen@chemie.uni-frankfurt.de
Matthias.Wagner@chemie.uni-frankfurt.de

Supporting information for this article is available on the WWW under http://dx.doi.org/10.1002/chem.200800588: Crystallographic characterization of **3** and **7**; view of the polymeric structure of K[**5**]; cyclic voltammograms of K[**5**] and K[**11**]; illustration of the sterically hindered interconversion of $[Cu^I(N_4)^{tet}]^-$ and $[Cu^{II}(N_4)^{spl}]$; comparison of calculated structures with X-ray data; atomic coordinates and total energies of all optimized structures.

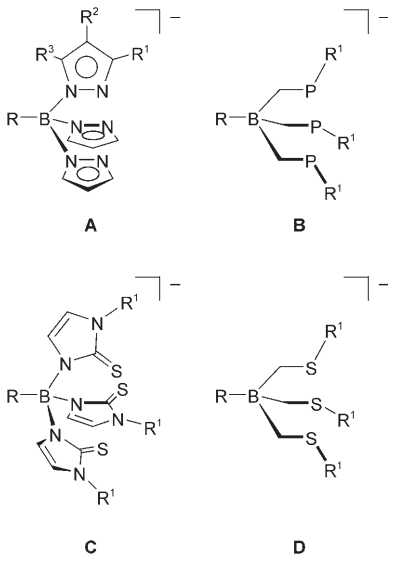


Figure 1. Tridentate facially coordinating borate ligands **A**–**D** (substituents $R^1$–$R^3$ on two pyrazolyl rings of **A** not shown).

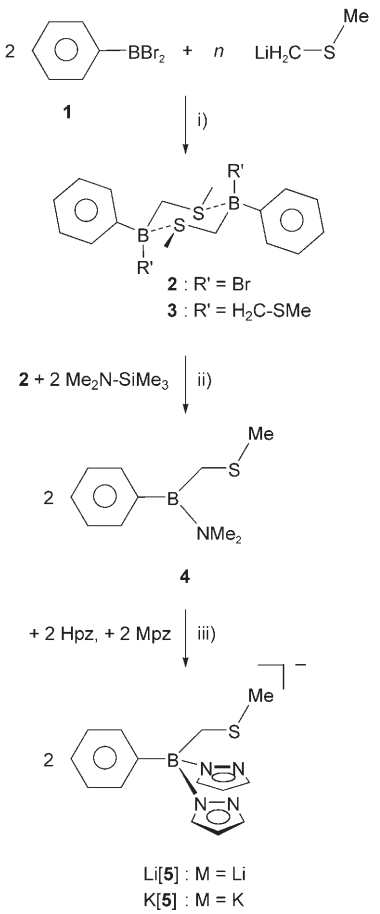


Scheme 1. Synthesis of the 1,4-dimethyl-1,4-dithionia-2,5-diboratacyclohexanes **2**/**3** and of the ($N_2S$) scorpionate salts Li[**5**]/K[**5**]. i) **2**: $n=2$, **3**: $n=4$; $C_6H_6$, 6 °C→RT, ii) $C_6H_6$, 6 °C→RT, iii) toluene, reflux.

(($N_2P$),[13,14] ($NP_2$)[15]) or nitrogen and sulfur donors (($N_2S$),[16] ($NS_2$)[17–22]). These derivatives are most interesting, because they allow a smooth modulation of the coordination environment between the extremes ($N_3$) and ($P_3$)/($S_3$). Complete homogeneous series of closely related ligands facilitate an evaluation of the influence of gradual changes in the donor set of tripods on the chemical properties of the coordinated metal ion. This has been impressively demonstrated by Vahrenkamp et al., who compared the biomimetic thiolate-alkylating activity of tetrahedral (tet) zinc complexes supported by $[HBpz_x(thioimidazolyl)_{3-x}]^-$ (pz = pyrazol-1-yl) ligands upon variation of $x$ from $x=0$ to 3.[23–26] For our own research on bioinorganic model systems with mixed-donor scorpionates $[RBpz_x(S\text{-donor})_{3-x}]^-$ we prefer (methylthio)-methyl- over thioimidazolyl groups, because different substituents linked to the same boron center through B–N and B–C bonds are less likely to scramble than substituents that are all bonded through $sp^2$-hybridized nitrogen atoms. Unfortunately, in the case of the thioether scorpionates $[RBpz_x(CH_2SR^1)_{3-x}]^-$ the homogeneous series is incomplete, because derivatives $[RBpz_2(CH_2SR^1)]^-$ are lacking. It was therefore necessary to develop a facile route to these missing members, and a high-yield synthesis of the derivative $[PhBpz_2(CH_2SMe)]^-$ will be described in this paper ([**5**]$^-$; Scheme 1).

The potential of scorpionates $[RBpz_x(CH_2SR^1)_{3-x}]^-$ goes far beyond the preparation of mononuclear complexes, because they can be tied to other ligands through their non-coordinating substituent R. In the past, our group has spent considerable effort developing ditopic scorpionates which we have used for the assembly of coordination polymers,[27,28] multiple-decker sandwich complexes,[29–31] metallo-macrocycles[32] and dinuclear complexes with cooperating metal ions.[33–35] So far, the main focus was on *homo*ditopic ligand systems consisting of two identical scorpionate units that are bridged by organometallic or aromatic linkers. Replacement of pyrazolyl rings by thioether moieties allows to extend the research to *hetero*ditopic scorpionate ligands in which the two donor sites are no longer the same so that the two coordinated metal centers will show different reactivity.

Our choice of the first heteroditopic target scorpionate for bioinorganic research projects was guided by the idea that it should be similar to the ligand environment of naturally occurring dinuclear metalloproteins for which the added value of the second metal ion is already proven. In this respect, the two copper-containing enzymes dopamine β-monooxygenase (DβM) and peptidylglycine α-hydroxylating monooxygenase (PHM) appeared to be particularly attractive, because each of them contains two copper ions separated by approximately 11 Å, one with three histidine-imidazolyl ligands ($Cu_H$) and the other bonded to two imidazoles and a methionine-thioether chain ($Cu_M$).[36–38] DβM and PHM catalyze stereospecific hydroxylations of C–H bonds in the biosynthetic pathways of norepinephrine and α-amidated peptides, respectively. $Cu_M$ is the presumed site of dioxygen binding, whereas the role of $Cu_H$ is merely that of an electron source.[37,39]

  

The coordination spheres of $Cu_H$ and $Cu_M$ can be nicely modeled by $[RBpz_3]^-$ and $[RBpz_2(CH_2SMe)]^-$ ligands, respectively.[40] Connection of the two fragments by a *p*-phenylene linker would result in the heteroditopic scorpionate $[\mathbf{10}]^{2-}$ (Scheme 2), which, in its straight conformation, supports a metal–metal distance of about 11 Å as it has been found in DβM and PHM.

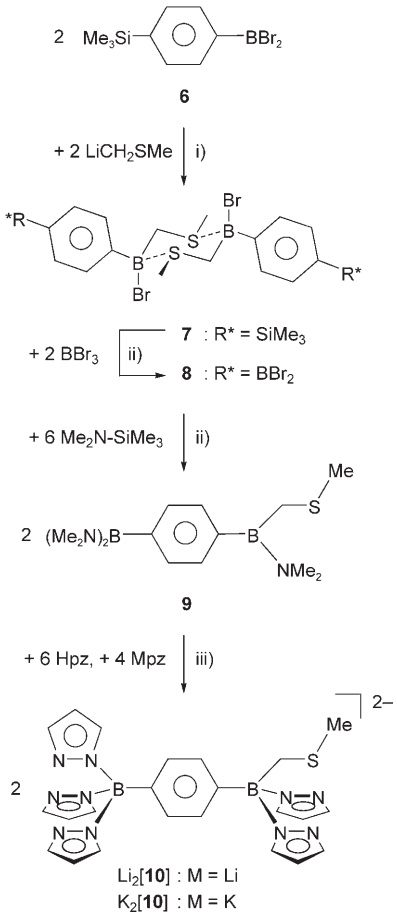


Scheme 2. Synthesis of the heteroditopic scorpionate ligands $Li_2[\mathbf{10}]$ and $K_2[\mathbf{10}]$. i) $C_6H_6$, 6 °C→RT, ii) $C_6H_6$, RT, iii) toluene, reflux.

Given this background, we have prepared the monotopic scorpionate $[PhBpz_2(CH_2SMe)]^-$ ($[\mathbf{5}]^-$) and characterized its $Cu^I$ and $Cu^{II}$ complexes. Based on these results, we have further developed this chemistry to the point where a targeted synthesis of the first heteroditopic scorpionate ligand *p*-$[pz_3B–C_6H_4–Bpz_2(CH_2SMe)]^{2-}$ ($[\mathbf{10}]^{2-}$) was possible and we have studied the coordination behavior of $[\mathbf{10}]^{2-}$ towards $Cu^I$ ions.

## Results and Discussion

So far, ($S_3$) and ($NS_2$) borate ligands have been prepared by using efficient one-pot protocols.[9–11,18,19,41] With regard to our aim of developing a general route to heteroditopic thioether scorpionates, it was now inevitable to elucidate in detail the chemical and structural properties not only of the ligands themselves, but also of key intermediates.

**Syntheses**: The lithium and potassium ($N_2S$) scorpionates Li[**5**] and K[**5**] are accessible through a three-step sequence starting from $PhBBr_2$[42] (Scheme 1).

For the selective introduction of one or two (methylthio)-methyl groups in the first reaction step we employed donor-free $LiCH_2SMe$,[43] because, in our hands, it gave far better results than the corresponding TMEDA-adduct (TMEDA: tetramethylethylenediamine). The improvement in terms of selectivity and yield of **2** and **3** was so significant that it outweighed the hazards associated with working with donor-free $LiCH_2SMe$ (the compound violently explodes upon air contact[43]). One advantage of the TMEDA-free reagent lies in its poor solubility in the reaction solvent ($C_6H_6$) which guarantees low stationary concentrations of the nucleophile and makes it easier to control whether mono- (**2**) or disubstitution (**3**) takes place. Moreover, removal of LiBr during workup is greatly facilitated if TMEDA is absent. According to X-ray crystallography and NMR spectroscopy, both **2** and **3** form dimers in the solid state as well as in solution. Irrespective of that, addition of $Me_2NSiMe_3$ to **2** resulted in the clean formation of the monomeric aminoborane **4**. The borate salts Li[**5**] and K[**5**] were finally obtained by transamination of **4** with a mixture of pyrazole and alkali metal pyrazolide. Another hybrid ligand, Riordan's[18] ($NS_2$) scorpionate $Li[PhBpz(CH_2SMe)_2]$, was accessible from **3** and lithium pyrazolide (Lipz).

For the synthesis of the heteroditopic scorpionates $Li_2[\mathbf{10}]$ and $K_2[\mathbf{10}]$ the *p*-silylated borylbenzene **6**[44,45] was chosen as starting material (Scheme 2). Introduction of the thioether substituent by using donor-free $LiCH_2SMe$ gave the silylated analog (**7**) of **2**. Similar to **2**, **7** exists as dimer in solution and in the solid state (see the Supporting Information). This is of critical importance for the entire synthesis concept, because B–S adduct formation protects the thioether groups from $BBr_3$ attack in the subsequent reaction step, thereby allowing the clean conversion of **7** into **8** via silicon/boron exchange. Treatment of **8** with 6 equiv of $Me_2NSiMe_3$ led to the replacement of all bromide substituents by dimethylamino groups and consequently to the break-up of the 1,4-dithionia-2,5-diboratacyclohexane ring. The resulting monomer **9** was transformed into the heteroditopic scorpionates $Li_2[\mathbf{10}]$ and $K_2[\mathbf{10}]$ by reaction with Hpz/Mpz (6:4; M = Li, K) in toluene at reflux temperature.

The copper complexes K[**11**] and **12** (Scheme 3) were prepared by the reaction of K[**5**] with 1.3 equiv of CuCl and 0.5 equiv of $CuBr_2$, respectively. Toluene was chosen as the reaction medium, which led to heterogeneous conditions and thus to reaction times of several days. The solubility of K[**5**] in toluene is higher than the solubility of CuCl, thus promoting the formation of complexes of stoichiometry $K[Cu(\mathbf{5})_2]$ (i.e., K[**11**]), even though the ratio of the starting materials was roughly 1:1. Samples prepared in solvents

  

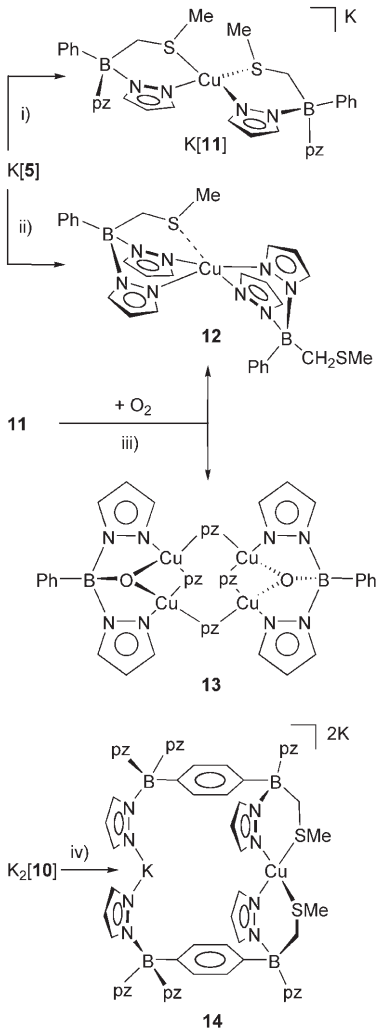


Scheme 3. Synthesis of the mononuclear $Cu^{I}$ and $Cu^{II}$ complexes K[**11**] and **12**, the tetranuclear species **13**, and of the dinuclear $K^{+}/Cu^{I}$ complex **14**; the molecular structures are drawn according to the results of the X-ray crystal structure analyses. i) + CuCl, toluene, RT, ii) + $CuBr_2$, toluene, RT, iii) $C_6H_6$, RT, iv) + CuCl, THF, RT.

other than toluene did not provide single crystalline-material.

As already mentioned in the introductory part, copper complexes of the ($N_2S$) scorpionate ligand $[\mathbf{5}]^-$ can be regarded as mimics of the $O_2$-activating copper site in the hydroxylating enzymes DβM and PHM. We therefore investigated the behavior of K[**11**] towards dry molecular oxygen in $C_6H_6$ solution at room temperature. From the paramagnetic reaction mixture, crystals were grown of the $Cu^{II}$ complex **12** (major component) and of a degradation product **13** containing $[PhBpz_2(O)]^{2-}$ ligands (minor component; Scheme 3). The oxidative cleavage of the B–C bond indicates activation of $O_2$ by K[**11**] in a manner reminiscent of related enzyme-mediated processes. The heterodinuclear complex **14** (Scheme 3) was synthesized from $K_2$[**10**] and CuCl in THF (stoichiometric ratio = 1:3).

**Spectroscopy**: The $^{11}$B NMR spectrum of **2** shows one resonance at 2.5 ppm testifying to the presence of four-coordinated boron nuclei.[46] This result can best be explained by assuming that a B–S adduct is present in $C_6D_6$ solution. Owing to the self-complementarity of $PhB(Br)CH_2SMe$ and entropy reasons, the structure of this adduct is most likely that of a cyclic dimer $(PhB(Br)CH_2SMe)_2$ (Scheme 1). The $BCH_2$ protons of **2** are not magnetically equivalent, but give rise to two doublets (each integrating to 2H) in the $^1$H NMR spectrum, which is in accord with the presence of chiral boron centers in $(PhB(Br)CH_2SMe)_2$ ($\delta(^1H) = 2.64$, 2.08 ppm; $^2J(H,H) = 12.7$ Hz). The corresponding $BCH_2$ carbon atoms lead to only one resonance (at $\delta = 34.9$ ppm) that is considerably broadened, owing to unresolved $^1J(B,C)$ coupling and fast quadrupolar relaxation of the boron nuclei. Only one set of phenyl and methyl signals is observed in the $^1$H and $^{13}$C NMR spectra of **2**, thus ruling out the presence of more than one of the possible isomers resulting from different distributions of the substituents over the axial/equatorial positions of the 1,4-dithionia-2,5-diboratacyclohexane ring.

Similar to **2**, the triorganylborane **3** reveals one $^{11}$B resonance at $\delta = -4.7$ ppm and is therefore also likely to exist as B–S adduct in solution. In contrast to **2**, the $^1$H and $^{13}$C NMR spectra of **3** are rather complex and difficult to assign because of many broadened and overlapping signals. If we again assume a 1,4-dithionia-2,5-diboratacyclohexane structure, one part of the problem clearly arises from the two different $CH_2SMe$ fragments present in the molecule. In addition, different isomers may exist in parallel or slowly transform into each other in $C_6D_6$ solution. We therefore added pyridine to the NMR tube in order to cleave the B–S adducts and to form $PhB(CH_2SMe)_2$·py complexes instead. As a result, the $^{11}$B NMR signal was shifted downfield to 0.0 ppm and the $^1$H NMR spectrum simplified considerably and showed a better resolution. All in all, we observe three resonances for the phenyl ring, three for the coordinated pyridine molecule, and one signal for the SMe groups. The corresponding integral ratio of 5:5:6 gives conclusive evidence for the proposed structure. The $BCH_2$ protons are still inequivalent ($\delta(^1H) = 2.55$, 2.44 ppm; $^2J(H,H) = 11.9$ Hz), because the boron atom of $PhB(CH_2SMe)_2$·py is prochiral.

The $^{11}$B NMR spectrum of the aminoborane **4** is characterized by one signal at $\delta = 40.6$ ppm that lies in a range typical of three-coordinated boron atoms.[46] N–B π-bonding apparently reduces the Lewis acidity of the boron center to such an extent that no B–S adducts are formed anymore. This view is supported by the observation of two singlets in the $^1$H NMR spectrum that are assignable to the $NMe_2$ group and point towards a hindered rotation about the B–N bond as a result of significant double bond character ($\delta(^1H) = 2.64$, 2.47 ppm; $\delta(^{13}C) = 41.0$, 39.7 ppm). The proton resonance of the $BCH_2$ fragment appears as one singlet at $\delta(^1H) = 2.22$ ppm.

In line with the proposed borate structure of Li[**5**], its $^{11}$B resonance possesses a chemical shift value of −0.8 ppm. Pyr-

  

azolyl resonances are observed at $\delta(^1H) = 8.18$, 7.45, 6.14 ppm and $\delta(^{13}C) = 139.3$, 135.8, 102.9 ppm. The integral ratio of the Ph, pz, and $CH_2SMe$ signals in the proton spectrum of Li[**5**] fits to a (methylthio)methyl-bis(pyrazol-1-yl)-borate ion. All key NMR data of K[**5**] are similar to those of Li[**5**] and therefore do not merit a detailed discussion.

The NMR data of **7** closely resemble those of **2**, apart from the fact that the proton resonances of the aromatic ring now give a well-resolved AA′BB′ pattern ($\delta(^1H) = 7.94$, 7.59 ppm; $\delta(^{13}C) = 133.4$, 132.8 ppm) and that a $SiMe_3$ signal appears at $\delta(^1H) = 0.27/\delta(^{13}C) = -1.0$ ppm. The successful replacement of $SiMe_3$ by $BBr_2$ in **8** is evident from the disappearance of the $SiMe_3$ signals accompanied by a downfield shift of *p*-phenylene resonances, owing to the π-electron withdrawing nature of the dibromoboryl substituent ($\delta(^1H) = 8.16$, 7.74 ppm; $\delta(^{13}C) = 137.5$, 132.9 ppm). Somewhat surprisingly, no $^{11}B$ NMR signal was detectable for the $BBr_2$ group in **8** ([$D_8$]toluene; four-coordinated boron atom: $\delta(^{11}B) = 2.2$ ppm). This problem is solved after amination, because **9** gives rise to two $^{11}B$ NMR signals with an integral ratio of 1:1 and chemical shift values of 40.7 and 33.1 ppm. Characteristically, the four methyl groups of the $B(NMe_2)_2$ fragment are all equivalent at room temperature ($\delta(^1H) =$ 2.64 ppm (12H); $\delta(^{13}C) = 41.3$ ppm), whereas those of the $B(NMe_2)(CH_2SMe)$ moiety appear as two singlets with $\delta(^1H) = 2.69$ (3H)/2.57 ppm (3H) and $\delta(^{13}C) = 41.2$/39.8 ppm. This well-known feature is usually attributed to resonance saturation and thus to a lower degree of N–B π-bonding in the $B(NMe_2)_2$ case.

For the heteroditopic scorpionates $Li_2$[**10**] and $K_2$[**10**] we note NMR spectra that are merely a superposition of the spectra of $[PhBpz_3]^-$[47] and [**5**]$^-$. Resonances for the *p*-phenylene bridge are observed at $\delta(^1H) = 6.42$–6.30 ($Li_2$[**10**])/ 7.02–6.89 ppm ($K_2$[**10**]) and at $\delta(^{13}C) = 132.3$, 131.1 ($Li_2$[**10**])/ 133.6, 133.0 ppm ($K_2$[**10**]).

The room temperature $^1H$ and $^{13}C$ NMR spectra of the $Cu^I$ complex K[**11**] are characterized by broad and ill-defined signals. Much sharper and interpretable resonances are, however, obtained if the sample is heated to +50 °C. This clearly indicates motional broadening rather than paramagnetic $Cu^{II}$ impurities to be responsible for the poor resolution of the room temperature spectra of K[**11**]. At +50 °C, only one set of signals is observed for the pyrazolyl protons and all $BCH_2$ protons have the same chemical shift value. These observations are not compatible with a static molecular structure, but rather point towards association/dissociation equilibria in solution. We note, however, that the NMR data of K[**11**] at elevated temperature are still decisively different from those of the free ligand [**5**]$^-$. Owing to their paramagnetic nature, no interpretable NMR data of the $Cu^{II}$ complexes **12** and **13** were obtained. In the case of the $Cu^I$ complex **14**, the yield of single crystalline material was very low so that the entire sample was consumed in the selection of an appropriate specimen for X-ray crystallography.

**X-Ray crystal structure analyses**: The compounds **2**, **3**, ($Li$[**5**])$_2$, K[**5**], **7**, $K_2$[**10**](thf)$_2$, (K[**11**])$_2$, **12**, **13**, and **14**(thf)$_2$ were characterized by X-ray crystallography. Key crystallographic data are compiled in Tables 1 and 2 and Table 1S (**3**, **7**) in the Supporting Information).

Intermediate **2** crystallizes from pentane/$C_6H_6$ with two crystallographically independent molecules in the asymmet-

Table 1. Crystallographic data for **2**, ($Li$[**5**])$_2$, K[**5**] and $K_2$[**10**](thf)$_2$.

| | **2** | ($Li$[**5**])$_2$ | K[**5**] | $K_2$[**10**](thf)$_2$ |
|---|---|---|---|---|
| formula | $C_{16}H_{20}B_2Br_2S_2$ | $C_{28}H_{32}B_2Li_2N_8S_2$ | $C_{14}H_{16}BKN_4S$ | $C_{31}H_{40}B_2K_2N_{10}O_2S{\cdot}C_4H_8O$ |
| *fw* | 457.88 | 580.24 | 322.28 | 788.71 |
| color, shape | colorless, plate | colorless, block | colorless, needle | colorless, block |
| crystal size [mm] | 0.31×0.26×0.12 | 0.42×0.37×0.35 | 0.23×0.13×0.12 | 0.23×0.21×0.18 |
| *T* [K] | 173(2) | 173(2) | 173(2) | 173(2) |
| radiation [Å] | $MoK_\alpha$ 0.71073 | $MoK_\alpha$ 0.71073 | $MoK_\alpha$ 0.71073 | $MoK_\alpha$ 0.71073 |
| crystal system | triclinic | monoclinic | orthorhombic | triclinic |
| space group | $P\bar{1}$ | $P2_1/c$ | $P2_12_12_1$ | $P\bar{1}$ |
| *a* [Å] | 6.7169(7) | 8.4318(4) | 9.2358(7) | 11.6438(14) |
| *b* [Å] | 10.1354(12) | 10.3095(5) | 12.7378(11) | 12.6677(16) |
| *c* [Å] | 21.012(2) | 17.7212(8) | 13.8257(13) | 15.2056(17) |
| α [°] | 77.436(9) | 90 | 90 | 70.376(9) |
| β [°] | 81.911(8) | 97.510(3) | 90 | 79.682(9) |
| γ [°] | 82.653(9) | 90 | 90 | 86.565(10) |
| *V* [Å$^3$] | 1375.3(3) | 1527.25(12) | 1626.5(2) | 2078.4(4) |
| *Z* | 3 | 2 | 4 | 2 |
| $D_{calcd}$ [g cm$^{-3}$] | 1.659 | 1.262 | 1.316 | 1.260 |
| *F*(000) | 684 | 608 | 672 | 832 |
| μ[mm$^{-1}$] | 4.641 | 0.207 | 0.452 | 0.324 |
| no. of reflns collected | 10646 | 38150 | 10736 | 17462 |
| no. of indep reflns ($R_{int}$) | 4931 (0.0475) | 4254 (0.0348) | 3037 (0.0718) | 7748 (0.1079) |
| no. of reflns obsd ($I > 2\sigma(I)$) | 4065 | 4067 | 2374 | 4272 |
| no. of data/restraints/params | 4931/0/298 | 4254/0/191 | 3037/0/190 | 7748/114/478 |
| GOF on $F^2$ | 1.013 | 1.096 | 1.017 | 1.003 |
| *R*1, *wR*2 ($I > 2\sigma(I)$) | 0.0419, 0.1002 | 0.0606, 0.1704 | 0.0627, 0.1394 | 0.1001, 0.2601 |
| *R*1, *wR*2 (all data) | 0.0542, 0.1055 | 0.0626, 0.1722 | 0.0857, 0.1506 | 0.1576, 0.3059 |
| largest diff peak and hole (*e* Å$^{-3}$) | 0.825/−1.264 | 0.992/−0.655 | 0.533/−0.434 | 0.708/−0.371 |

Table 2. Crystallographic data for $(K[\mathbf{11}])_2$, **12**, **13** and $\mathbf{14}(thf)_2$.

| | $(K[\mathbf{11}])_2$ | **12** | **13** | $\mathbf{14}(thf)_2$ |
|---|---|---|---|---|
| formula | $C_{56}H_{64}B_4Cu_2K_2N_{16}S_4 \cdot 2\,C_6H_6$ | $C_{28}H_{32}B_2CuN_8S_2$ | $C_{36}H_{34}B_2Cu_4N_{16}O_2$ | $C_{54}H_{64}B_4CuK_3N_{20}O_2S_2 \cdot 2\,C_4H_8O$ |
| *fw* | 1494.21 | 629.90 | 998.57 | 1457.66 |
| color, shape | colorless, block | light violet, plate | dark blue, block | colorless, plate |
| crystal size [mm] | $0.22\times0.21\times0.17$ | $0.18\times0.13\times0.07$ | $0.24\times0.23\times0.19$ | $0.12\times0.11\times0.03$ |
| $T$ [K] | 173(2) | 173(2) | 173(2) | 173(2) |
| radiation [Å] | $MoK_\alpha$ 0.71073 | $MoK_\alpha$ 0.71073 | $MoK_\alpha$ 0.71073 | $MoK_\alpha$ 0.71073 |
| crystal system | triclinic | triclinic | monoclinic | monoclinic |
| space group | $P\bar{1}$ | $P\bar{1}$ | $P2_1/n$ | $C2/c$ |
| $a$ [Å] | 10.3367(6) | 9.9336(15) | 13.0380(9) | 28.393(4) |
| $b$ [Å] | 11.6603(7) | 10.2087(13) | 11.8504(11) | 15.3601(14) |
| $c$ [Å] | 31.508(2) | 16.917(3) | 13.0596(9) | 18.695(3) |
| $\alpha$ [°] | 81.959(5) | 90.134(12) | 90 | 90 |
| $\beta$ [°] | 81.978(5) | 98.521(13) | 103.699(5) | 117.551(10) |
| $\gamma$ [°] | 81.510(5) | 114.819(10) | 90 | 90 |
| $V$ [Å$^3$] | 3691.6(4) | 1535.9(4) | 1960.4(3) | 7228.7(17) |
| $Z$ | 2 | 2 | 2 | 4 |
| $D_{calcd}$ [g cm$^{-3}$] | 1.344 | 1.362 | 1.692 | 1.339 |
| $F(000)$ | 1552 | 654 | 1008 | 3048 |
| $\mu$[mm$^{-1}$] | 0.854 | 0.880 | 2.198 | 0.592 |
| no. of reflns collected | 44320 | 12355 | 12130 | 20283 |
| no. of indep reflns ($R_{int}$) | 14312 (0.0798) | 5395 (0.0857) | 3617 (0.0476) | 6372 (0.1449) |
| no. of reflns obsd ($I>2\sigma(I)$) | 10089 | 2622 | 3052 | 2410 |
| no. of data/restraints/params | 14312/0/865 | 5395/0/370 | 3617/0/271 | 6372/0/435 |
| GOF on $F^2$ | 1.143 | 0.947 | 1.017 | 0.870 |
| $R1$, $wR2$ ($I>2\sigma(I)$) | 0.0969, 0.2352 | 0.0809, 0.1709 | 0.0336, 0.0815 | 0.0824, 0.1259 |
| $R1$, $wR2$ (all data) | 0.1242, 0.2434 | 0.1692, 0.2075 | 0.0446, 0.0857 | 0.2194, 0.1691 |
| largest diff peak and hole ($e$ Å$^{-3}$) | 1.207/−0.687 | 1.133/−0.618 | 0.363/−0.524 | 0.909/−0.383 |

ric unit. One has $C_1$ symmetry, the other possesses an inversion center. All key structural parameters of the two molecules are the same within the margins of experimental error. Thus, only the $C_i$ symmetric structure will be discussed here (Figure 2).

As already deduced from its NMR spectra, compound **2** is indeed a 1,4-dithionia-2,5-diboratacyclohexane derivative. The six-membered heterocycle adopts a chair conformation in the solid state. Both bromide substituents occupy axial positions, whereas the sterically more demanding phenyl rings as well as the methyl groups are located at equatorial positions. The only other structurally characterized example of a 1,4-dithionia-2,5-diboratacyclohexane was reported by Nöth, who prepared the compound $(BH_2(CH_2SMe))_2$ by thermolysis of the amine adduct $Me_3N{\cdot}BH_2(CH_2SMe)$.[48] According to X-ray crystallography, $(BH_2(CH_2SMe))_2$ also prefers a chair conformation with two equatorial methyl substituents in the crystal lattice. NMR spectroscopy, however, indicated the presence of two conformational isomers, *trans*-(eq,eq) and *trans*-(ax,ax), in solution. The comparison of **2** with $(BH_2(CH_2SMe))_2$ revealed two differences in their molecular structures: First, the B–S adduct bonds of **2** are significantly longer (2.000(5) Å vs. 1.951(2) Å) and second, the S–B–C and B–S–C bond angles are the same in **2** (S(3)–B(3)–C(3$^{\#}$) = 105.5(3)°, B(3)–S(3)–C(3) = 104.5(2)°) but deviate from each other by 5.8° in $(BH_2(CH_2SMe))_2$ (108.1(1)°, 102.3(1)°). The B–S bond in **3** is elongated even further to a value of 2.029(3) Å, although the B–S bond in **7** is 1.972(10) Å long (see the Supporting Information, Figures 1aS and 1bS).

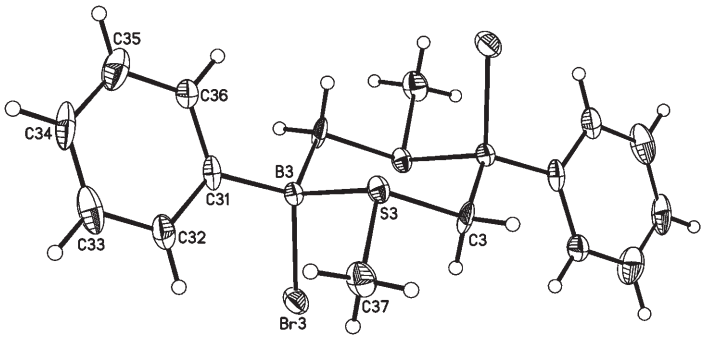


Figure 2. Molecular structure of **2** in the solid state; thermal ellipsoids at the 50% probability level. Selected bond lengths [Å], bond angles [°], torsion angles [°], and dihedral angles [°]: B(3)–S(3) 2.000(5), B(3)–C(3$^{\#}$) 1.641(6), B(3)–C(31) 1.610(6), B(3)–Br(3) 2.065(5), S(3)–C(3) 1.812(4), S(3)–C(37) 1.811(5); S(3)–B(3)–C(3$^{\#}$) 105.5(3), B(3)–S(3)–C(3) 104.5(2), B(3)–S(3)–C(37) 104.9(2), C(3)–S(3)–C(37) 102.1(2); B(3)–S(3)–C(3)–B(3$^{\#}$) 66.1(4), C(3$^{\#}$)–B(3)–S(3)–C(37) −168.5(3), C(31)–B(3)–S(3)–C(37) 70.3(3), Br(3)–B(3)–S(3)–C(37) −50.8(3); C(3$^{\#}$)B(3)S(3)//C(3)S(3)C(3$^{\#}$)S(3$^{\#}$) 58.3. Symmetry transformation used to generate equivalent atoms: #: $-x+1, -y+1, -z+2$.

The lithium scorpionate complex Li[**5**] crystallizes in the form of centrosymmetric dimers $(Li[\mathbf{5}])_2$ (Figure 3).

Each $Li^+$ ion has a distorted tetrahedral ligand environment consisting of two pyrazolyl rings of one borate ligand together with one pyrazolyl ring and the (methylthio)methyl group of the other ligand. Two of the four pyrazolyl donors within the aggregate adopt bridging positions between $Li^+$ ions. The entire structure is strongly reminiscent of the mo-

  

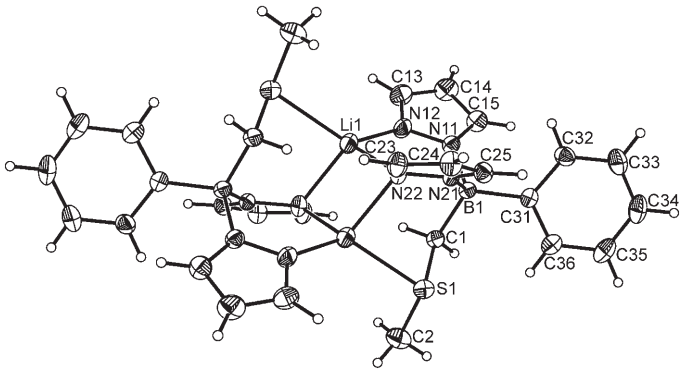


Figure 3. Molecular structure of $(Li[\mathbf{5}])_2$ in the solid state; thermal ellipsoids at the 50% probability level. Selected bond lengths [Å], bond angles [°], and torsion angles [°]: Li(1)–N(12) 1.960(4), Li(1)–N(22) 2.115(4), Li(1)–N(22$^{\#}$) 2.160(4), Li(1)–S(1$^{\#}$) 2.498(3), B(1)–N(11) 1.579(2), B(1)–N(21) 1.586(2), B(1)–C(1) 1.641(3), B(1)–C(31) 1.626(3), S(1)–C(1) 1.804(2), S(1)–C(2) 1.815(2), Li(1)···Li(1$^{\#}$) 2.624(7); N(12)–Li(1)–N(22) 96.5(2), N(22$^{\#}$)–Li(1)–S(1$^{\#}$) 88.8(1), Li(1)–N(22)–Li(1$^{\#}$) 75.7(2), N(22)–Li(1)–N(22$^{\#}$) 104.3(2), N(11)–B(1)–N(21) 107.7(1), N(21)–B(1)–C(1) 109.7(1); B(1)–N(11)–N(12)–Li(1) 16.3(3), B(1)–N(21)–N(22)–Li(1) –33.2(2), B(1)–N(21)–N(22)–Li(1$^{\#}$) 54.4(2), B(1)–C(1)–S(1)–Li(1$^{\#}$) 83.3(2). Symmetry transformation used to generate equivalent atoms: #: $-x+1, -y+2, -z+1$.

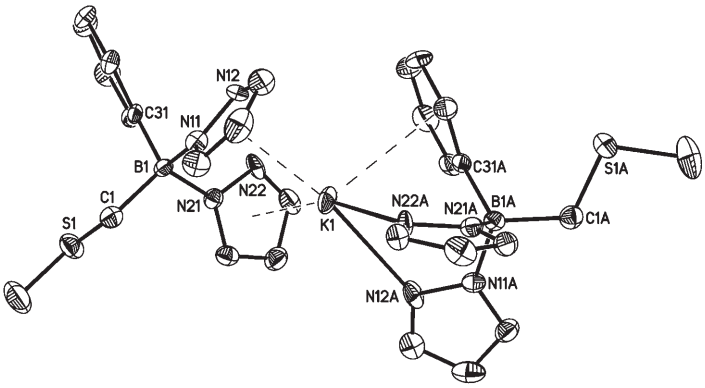


Figure 4. Section of the polymeric structure of K[**5**] in the solid state; thermal ellipsoids at the 50% probability level. The H atoms have been omitted for clarity. Selected bond lengths [Å], bond angles [°], and torsion angles [°]: K(1)–N(12 A) 2.871(5), K(1)–N(22 A) 2.840(5), K(1)–C(31 A) 3.054(4), K(1)–COG(pzN(11)) 3.000, K(1)–COG(pzN(21)) 2.971; N(11)–B(1)–N(21) 106.0(3), C(1)–B(1)–C(31) 112.3(4), N(12 A)–K(1)–N(22 A) 69.0(1); C(32)–C(31)–B(1)–C(1) 85.4(5). Symmetry transformation used to generate equivalent atoms: A: $x-1/2, -y+1/2, -z$.

lecular framework of the related dimer $(Li[FcBpz_3])_2$, apart from the fact that in the latter case ferrocenyl substituents (Fc) and pyrazolyl rings are occupying the positions of the phenyl and (methylthio)methyl groups, respectively.[28] Important bond lengths of $(Li[\mathbf{5}])_2$ are Li(1)–S(1$^{\#}$) = 2.498(3) Å, Li(1)–N(12) = 1.960(4) Å, and Li(1)–N(22) = 2.115(4) Å/Li(1)–N(22$^{\#}$) = 2.160(4) Å. Comparable Li–S bond lengths have been reported for the dimeric compound $(Li(TMEDA)[CH_2SPh])_2$ (six-membered ring; Li–S = 2.555(3) Å[49]), the polymeric aggregate $(Li(thf)[CH_2SMe])_\infty$ (ladder-like structure; Li–S = 2.531(5) Å[50]), and the infinite network of solvent-free (methylthio)methyllithium (Li–S = 2.443(13) Å/2.662(12) Å[43]). The phenomenon of considerably shorter Li–N bonds to the $\eta^1$-coordinating pyrazolyl rings compared to bonds between $Li^+$ and μ-coordinating pyrazolyl donors has also been observed for $(Li[FcBpz_3])_2$.

The solid state structure of the $K^+$ complex K[**5**] is fundamentally different from that of the $Li^+$ complex $(Li[\mathbf{5}])_2$: First, K[**5**] is polymeric rather than dimeric in the crystal lattice (Figure 4, Figure 1cS in the Supporting Information). Second, the (methylthio)methyl chains are merely dangling side groups, not coordinated to $K^+$ ions in K[**5**]. Third, π-interactions involving both the phenyl and pyrazolyl rings contribute to the coordinative saturation of the $K^+$ centers.

A more detailed inspection of the bonding situation reveals that each $K^+$ ion interacts with one scorpionate ligand through its two pyrazolyl nitrogen atoms (σ-mode; K(1)–N(12 A) = 2.871(5) Å, K(1)–N(22 A) = 2.840(5) Å) and the phenyl ring (π-mode; shortest contact: K(1)–C(31 A) = 3.054(4) Å). A second borate ion functions as a chelating ligand using the π-faces of both pyrazolyl rings for $K^+$ coordination; the distances between the metal ion and the ring centroids (COG) amount to K(1)–COG(pzN(11)) = 3.000 Å and K(1)–COG(pzN(21)) = 2.971 Å.

The potassium salt of the heteroditopic scorpionate $K_2[\mathbf{10}]$ crystallizes from THF together with three solvent molecules. Two of them coordinate the two $K^+$ ions ($K_2[\mathbf{10}](thf)_2$), the third THF molecule occupies space in the crystal lattice without acting as a ligand. Similar to K[**5**], $K_2[\mathbf{10}](thf)_2$ establishes a polymeric structure in the solid state. A section of this polymer is shown in Figure 5.

Again similar to K[**5**], the phenylene ring of $K_2[\mathbf{10}](thf)_2$ takes part in potassium coordination so that an inverse sandwich complex is created in which two $K^+$ ions are bonded to the opposite sides of the same π-electron system (K(1)···COG(Ar) = 2.988 Å, K(2)···COG(Ar) = 3.045 Å; K(1)···COG(Ar)···K(2) = 164.6°). In addition to the phenylene ring and one THF ligand, potassium ion K(1) is coordinated to the pyrazolyl ring pzN(11) of the heteroscorpionate fragment and to pzN(31) of the homoscorpionate moiety (σ-modes; K(1)–N(12) = 2.856(5) Å, K(1)–N(32) = 2.910(6) Å). K(2) binds to pzN(51) (σ-mode; K(2)–N(52) = 3.389(5) Å) and to the thioether chain (K(2)–S(1) = 3.363(2) Å). The K–S interaction is remarkable, because (methylthio)methyl coordination does not occur in the monotopic derivative K[**5**]. Most interestingly, *trans*-chelation of the $K^+$ ions involving both scorpionate fragments is preferred over *cis*-chelation by either the tris(pyrazol-1-yl)borate or the [(methylthio)-methyl]borate ligand alone. The pyrazolyl rings pzN(21) and pzN(41) are not engaged in the coordination of K(1) or K(2), but bind to potassium ions of adjacent complexes (σ-modes). Additional short intermolecular contacts are established between these potassium ions and the π-faces of pzN(11)/pzN(51).

Compound K[**11**] contains two scorpionate ligands per $Cu^I$ ion. The monoanionic charge of the complex is balanced by a $K^+$ ion. Electrostatic attraction and the need for $K^+$ solvation lead to the formation of dimers $(K[\mathbf{11}])_2$ in the

  

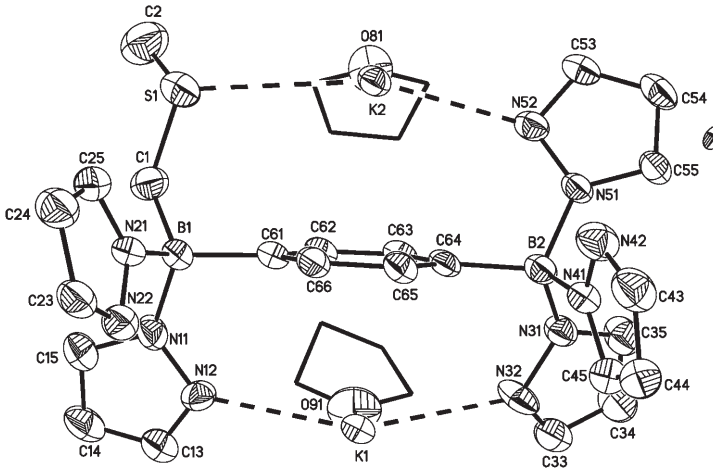


Figure 5. Section of the polymeric structure of $K_2$[**10**](thf)$_2$ in the solid state; thermal ellipsoids at the 50% probability level. For clarity, the H atoms have been omitted; the coordinated THF molecules are represented as sticks. Selected bond lengths [Å], bond angles [°], and torsion angles [°]: B(1)–C(1) 1.640(9), B(1)–C(61) 1.625(8), B(1)–N(11) 1.578(7), B(1)–N(21) 1.563(9), B(2)–C(64) 1.618(8), B(2)–N(31) 1.566(8), B(2)–N(41) 1.571(8), B(2)–N(51) 1.564(7), K(1)–N(12) 2.856(5), K(1)–N(32) 2.910(6), K(1)–O(91) 3.003(7), K(2)–N(52) 3.389(5), K(2)–O(81) 2.761(6), K(2)–S(1) 3.363(2), K(1)···COG($C_6H_4$) 2.988, K(2)···COG($C_6H_4$) 3.045; C(1)–B(1)–C(61) 112.4(5), C(1)–B(1)–N(11) 108.0(5), C(1)–B(1)–N(21) 109.4(5), N(12)–K(1)–N(32) 151.5(2), S(1)–K(2)–N(52) 156.4(1); B(1)–N(11)–N(12)–K(1) −3.3(9), B(1)–C(1)–S(1)–K(2) 46.4(6), B(2)–N(31)–N(32)–K(1) 24.5(8), B(2)–N(51)–N(52)–K(2) 26.8(7).

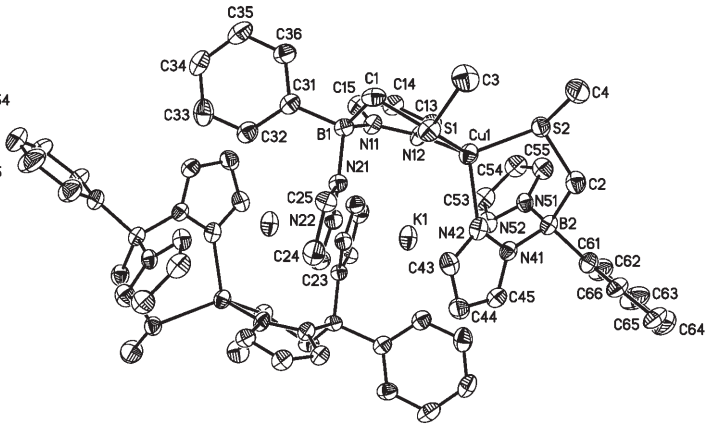


Figure 6. Molecular structure of one of the two crystallographically independent dimers (K[**11**])$_2$ in the solid state; thermal ellipsoids at the 50% probability level. The H atoms have been omitted for clarity. Selected bond lengths [Å], bond angles [°], and torsion angles [°]: Cu(1)–N(12) 2.054(7), Cu(1)–N(42) 2.058(7), Cu(1)–S(1) 2.251(2), Cu(1)–S(2) 2.267(2), K(1)–N(22) 2.851(7), K(1)–N(22$^{\#}$) 2.821(7), K(1)–N(52) 2.757(7), K(1)–N(12) 3.072(7); N(12)–Cu(1)–N(42) 108.5(3), N(12)–Cu(1)–S(1) 102.2(2), N(12)–Cu(1)–S(2) 104.5(2), N(42)–Cu(1)–S(1) 111.5(2), N(42)–Cu(1)–S(2) 101.3(2), S(1)–Cu(1)–S(2) 127.7(1), C(1)–S(1)–Cu(1) 104.0(3), C(2)–S(2)–Cu(1) 101.9(3), B(1)···Cu(1)···B(2) 140.9(2); B(1)–N(11)–N(12)–Cu(1) −4.2(11), B(1)–C(1)–S(1)–Cu(1) 48.2(6), B(2)–N(41)–N(42)–Cu(1) 17.4(10), B(2)–C(2)–S(2)–Cu(1) 54.9(7). Symmetry transformation used to generate equivalent atoms: #: $-x+2, -y+1, -z$.

solid state; two crystallographically independent, centrosymmetric dimers constitute the asymmetric unit of the crystal lattice. Since both dimers have similar bond lengths and angles, only one of them will be described here (Figure 6).

Each $Cu^{I}$ center is coordinated by two thioether and two pyrazolyl groups (pzN(11), pzN(41)) in a distorted tetrahedral fashion (smallest/largest bond angle: N(42)–Cu(1)–S(2) = 101.3(2)° / S(1)–Cu(1)–S(2) = 127.7(1)°). The two other pyrazolyl rings (pzN(21), pzN(51)) act as donors towards K(1) (K(1)–N(22) = 2.851(7) Å, K(1)–N(52) = 2.757(7) Å). The ligand sphere of K(1) is further completed by the π-faces of pzN(11) and pzN(41). Importantly, pzN(21) occupies a bridging position between K(1) and the symmetry-related ion K(1$^{\#}$) and thus links the two halves of the dimer together (K(1$^{\#}$)–N(22) = 2.821(7) Å). Copper ions surrounded by an ($N_2S_2$) ligand sphere as in (K[**11**])$_2$ occur naturally in so-called "blue copper proteins" that are functional in the reversible electron transfer: $Cu^{I} \rightleftarrows Cu^{II} + e^{-}$.[38,51–53] Crystal structures of these proteins show a very irregular tetrahedral coordination with two sulfur atoms from methionine and cysteinate and two histidine nitrogen atoms.[54] Numerous $Cu^{I}$ and $Cu^{II}$ complexes of mixed N- and S-donor ligands have been investigated as mimics of blue copper proteins to understand their intricate spectroscopical, electrochemical and structural features. We have selected representative examples with imine- and thioether-containing macrocyclic or thiosalen-type ligands for a structural comparison with (K[**11**])$_2$. These compounds exhibit Cu–N bond lengths in the range from 1.95 Å to 2.05 Å and Cu–S bond lengths between 2.21 Å and 2.29 Å,[55,56] which agree nicely with the corresponding bond lengths in (K[**11**])$_2$ (Cu(1)–N(12) = 2.054(7) Å, Cu(1)–N(42) = 2.058(7) Å, Cu(1)–S(1) = 2.251(2) Å, Cu(1)–S(2) = 2.267(2) Å).

The ligand/metal ratio of 2:1 present in the $Cu^{I}$ complex (K[**11**])$_2$ is retained in the $Cu^{II}$ complex **12** (Figure 7). How-

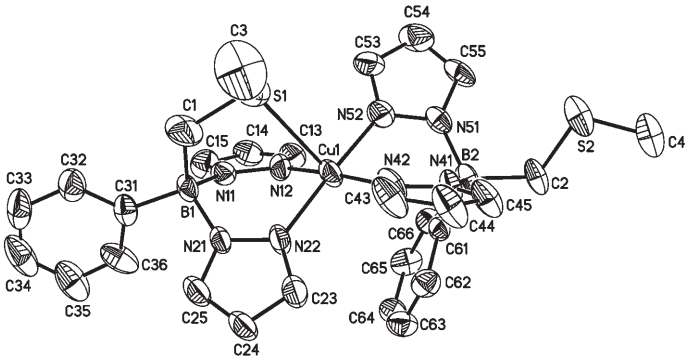


Figure 7. Molecular structure of **12** in the solid state; thermal ellipsoids at the 50% probability level. The H atoms have been omitted for clarity. Selected bond lengths [Å], bond angles [°], and torsion angles [°]: Cu(1)–N(12) 2.009(7), Cu(1)–N(22) 1.999(6), Cu(1)–N(42) 1.980(7), Cu(1)–N(52) 1.986(6), Cu(1)–S(1) 2.805(3); N(12)–Cu(1)–N(22) 88.4(2), N(12)–Cu(1)–N(42) 172.5(3), N(12)–Cu(1)–N(52) 90.0(3), N(42)–Cu(1)–N(52) 88.4(3), N(12)–Cu(1)–S(1) 83.1(2), N(22)–Cu(1)–S(1) 90.1(2), C(1)–S(1)–Cu(1) 98.7(3), B(1)···Cu(1)···B(2) 168.1(1); B(1)–N(11)–N(12)–Cu(1) −1.5(9), B(1)–N(21)–N(22)–Cu(1) -1.8(10), B(1)–C(1)–S(1)–Cu(1) −15.7(8), B(2)–N(41)–N(42)–Cu(1) −0.9(9), B(2)–N(51)–N(52)–Cu(1) 5.6(9).

  

ever, we observe a distinctly different coordination pattern with four pyrazolyl donors and one (methylthio)methyl group spacedly disposed at the corners of a slightly distorted square pyramid (trigonality index $\tau$[57] = 0.05).

Most importantly, the sulfur atom occupies the axial position. This feature makes compound **12** rather unique among the few structurally characterized $[Cu^{II}(sp^2\text{-}N)_4(SR_2)]^{n+}$ complexes, which are either square pyramidal (spy), but have the sulfur atom in an equatorial position,[58] or adopt a trigonal bipyramidal conformation[58,59] (again with the sulfur donor in an equatorial position). Thus, compound **12** fills a gap in the series of blue copper protein model systems, because an axially coordinated thioether donor in trigonal (bi)pyramidal active site geometries is suggested to confer highly positive $Cu^I/Cu^{II}$ redox potentials.[58,60] As a specific example of blue copper proteins, we are considering the dimensions of the copper site in poplar $Cu^{II}$-plastocyanin, which has the methionine sulfur atom located at a long but yet bonding distance of 2.82 Å to the $Cu^{II}$ ion.[54] This value compares nicely to the Cu(1)–S(1) bond length in complex **12** (2.805(3) Å). In contrast, a much shorter Cu–S bond (2.372(3) Å) is observed in the square-pyramidal ($\tau$ = 0.26) $[Cu^{II}(sp^2\text{-}N)_4(SR_2)]^{2+}$ complex [Cu(pmtpm)(2,9-dmp)]$(ClO_4)_2$ featuring an *equatorial* thioether ligand (pmtpm = 2-pyridyl-*N*-(2′-methylthiophenyl)methyleneimine; 2,9-dmp = 2,9-dimethyl-1,10-phenanthroline).[58] The pronounced difference in Cu–S bond lengths between **12** and [Cu(pmtpm)-(2,9-dmp)]$(ClO_4)_2$ is most likely owed to the Jahn–Teller distortion generally exhibited by five- and six-coordinated $d^9$-complexes. With regard to the Cu–S distance, **12** is, therefore, better compared to the $Cu^{II}$ complex $[Cu(L)](NO_3)_2$ (L = 4,7-bis(3-aminopropyl)-1-thia-4,7-diazacyclononane) possessing four $sp^3$-nitrogen atoms at the base of a square pyramid and a thioether moiety at the axial position. However, the bond distance Cu–S = 2.561(1) Å of the latter compound[61] is still 0.244 Å shorter than in **12** which may be due to the short (methylthio)methyl tether of the scorpionate ligand that prevents a closer approach of the sulfur atom. This interpretation is supported by a view at the Cu–S vector in **12**, which deviates by 10.7° from the normal to the least-squares plane (r.m.s. deviation 0.038 Å) through Cu(1) and its four N ligands. The four Cu–N bond lengths range from Cu(1)–N(42) = 1.980(7) Å to Cu(1)–N(12) = 2.009(7) Å and are thus in good agreement with the corresponding values in the related five-coordinate $Cu^{II}$ complexes.[58,59] The molecular structures of K[**11**] and **12** are distinctly different. Since these differences can easily be explained by applying basic rules for interactions between hard and soft Lewis acids and bases, it is interesting to note that Meyer et al. have published a $Cu^{II}$ complex in which the metal ion is surrounded by two pyrazolide-N- and two thioether-S-atoms in a distorted square-planar (dspl) *cis*-($N_2S_2$) coordination sphere.[62] On principle, it would be possible to establish a similar ligand environment also for $[Cu^{II}(\mathbf{5})_2]$, simply by twisting the orthogonal planes S(1)/Cu(1)/N(12) and S(2)/Cu(1)/N(42) of (K[**11**])$_2$ into a coplanar arrangement upon oxidation. However, the experimentally determined structure of **12** appears to be sufficiently more favorable than the alternative ($N_2S_2$) coordination to outweigh the high degree of ligand redistribution that is required for the transition from K[**11**] to **12**.

After treatment of the $Cu^I$ complex K[**11**] with dry air, two products, the mononuclear $Cu^{II}$ complex **12** and the tetranuclear $Cu^{II}$ species **13** (Figure 8) could be isolated.

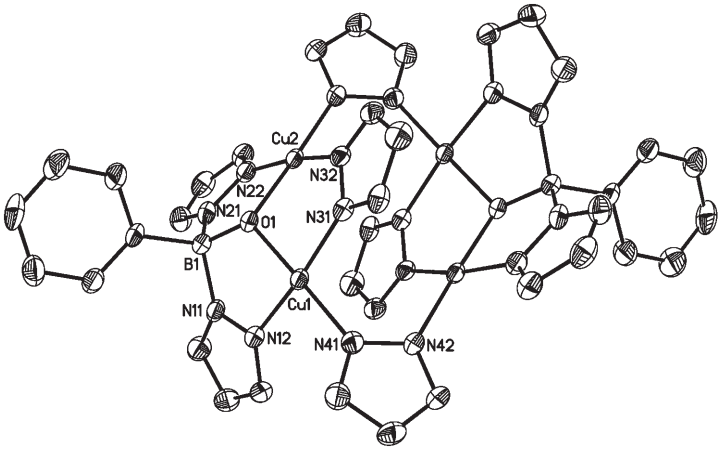


Figure 8. Molecular structure of **13** in the solid state; thermal ellipsoids at the 50% probability level. The H atoms have been omitted for clarity. Selected bond lengths [Å], bond angles [°], and torsion angles [°]: Cu(1)–O(1) 1.920(2), Cu(1)–N(12) 1.980(3), Cu(1)–N(31) 1.965(2), Cu(1)–N(41) 1.976(2), Cu(2)–O(1) 1.924(2), Cu(2)–N(22) 1.980(3), Cu(2)–N(32) 1.982(3), Cu(2)–N(42#) 1.973(2), B(1)–O(1) 1.443(4), B(1)–C(1) 1.626(4), B(1)–N(11) 1.595(4), B(1)–N(21) 1.578(4); Cu(1)–O(1)–Cu(2) 111.4(1), Cu(1)–O(1)–B(1) 117.1(2), Cu(2)–O(1)–B(1) 118.4(2), O(1)–Cu(1)–N(12) 84.5(1), O(1)–Cu(1)–N(31) 86.9(1), O(1)–Cu(1)–N(41) 178.9(1), N(12)–Cu(1)–N(31) 170.0(1), N(12)–Cu(1)–N(41) 94.5(1), N(31)–Cu(1)–N(41) 94.1(1), O(1)–Cu(2)–N(22) 84.3(1), O(1)–Cu(2)–N(32) 86.2(1), O(1)–Cu(2)–N(42#) 177.8(1), N(22)–Cu(2)–N(32) 170.4(1), N(22)–Cu(2)–N(42#) 94.0(1), N(32)–Cu(2)–N(42#) 95.6(1); B(1)–N(11)–N(12)–Cu(1) −13.2(3), B(1)–N(21)–N(22)–Cu(2) 2.3(3), Cu(1)–N(31)–N(32)–Cu(2) -0.4(2), Cu(1)–N(41)–N(42)–Cu(2#) 17.7(3). Symmetry transformation used to generate equivalent atoms: #: $-x+1$, $-y+1$, $-z+1$.

The formation of **13** is remarkable because not only have pyrazolide ions been released, but the (methylthio)methyl group has been replaced by an oxygen atom in the course of the reaction. Given the fact that we have taken all precautions to exclude moisture from the reaction mixture, the introduction of the oxygen atom into the scorpionate ligand is most likely the result of a $Cu^I$-mediated $O_2$ activation. This hypothesis is confirmed by the fact, that exposure of a toluene solution of the $Cu^{II}$ species **12** to air and moisture over a period of several weeks did not yield any indication for the formation of **13**. Again, we note that oxidative cleavage of the B–C-bond is reminiscent of the C–H activation achieved by the enzymes DβM and PHM. Once pyrazolylborates $[PhBpz_2(OH)]^-$ or $[PhBpz_2(O)]^{2-}$ have been formed, further degradation of these molecules with liberation of pyrazolide can easily occur because the three-coordinated boron atoms of the resulting fragments PhBpz(OH)/[PhBpz(O)]$^-$ are efficiently stabilized by O–B π donation.

  

Each half of the centrosymmetric molecule of **13** consists of one $[PhBpz_2(O)]^{2-}$ ligand that symmetrically bridges two $Cu^{II}$ ions by its oxygen atom (Cu(1)–O(1) = 1.920(2) Å, Cu(2)–O(1) = 1.924(2) Å).[63] The pyrazolyl nitrogen atom N(12) binds to Cu(1); N(22), which is part of the second pyrazolyl ring, coordinates Cu(2) (Cu(1)–N(12) = Cu(2)–N(22) = 1.980(3) Å). In addition to O(1), Cu(1) and Cu(2) are connected by a pyrazolide ion with Cu(1)–N(31) and Cu(2)–N(32) bond lengths of 1.965(2) Å and 1.982(3) Å, respectively. The square planar coordination sphere of each $Cu^{II}$ ion is completed by a second pyrazolide ligand that links the two halves of the tetranuclear aggregate (Cu(1)–N(41) = 1.976(2) Å, Cu(2#)–N(42) 1.973(2) Å).[64]

Complex **14** crystallized from a mixture of ligand $K_2$[**10**] and 3.3 equiv of CuCl in THF with one THF ligand bonded to each $K^+$ ion (**14**$(thf)_2$). The compound forms coordination polymers in the solid state; a view of the repeat unit, which possesses a $C_2$ axis running through Cu(1) and K(2), is provided in Figure 9.

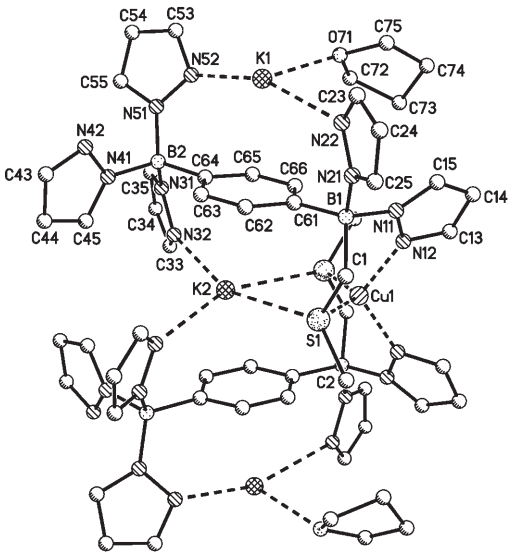


Figure 9. Molecular structure of **14**$(thf)_2$ in the solid state. For clarity, the H atoms have been omitted and atoms are represented as balls. Selected bond lengths [Å], bond angles [°], and torsion angles [°]: Cu(1)–S(1) 2.361(2), Cu(1)–N(12) 2.023(7), K(1)–N(22) 2.969(8), K(1)–N(52) 2.828(7), K(1)–O(71) 2.731(6), K(2)–N(32) 2.840(8), K(2)–S(1) 3.385(3), K(1)–COG($C_6H_4$) 3.033, K(2)–COG($C_6H_4$) 3.051; S(1)–Cu(1)–S(1#) 128.2(1), S(1)–Cu(1)–N(12) 98.8(2), S(1)–Cu(1)–N(12#) 109.6(2), N(12)–Cu(1)–N(12#) 112.0(4), N(22)–K(1)–N(52) 160.0(2), N(22)–K(1)–O(71) 86.6(2), N(52)–K(1)–O(71) 95.4(2); B(1)–N(11)–N(12)–Cu(1) –0.7(11), B(1)–C(1)–S(1)–Cu(1) 47.3(6), B(1)–N(21)–N(22)–K(1) 36.9(9), B(2)–N(31)–N(32)–K(2) -21.3(11), B(2)–N(51)–N(52)–K(1) –21.1(11). Symmetry transformation used to generate equivalent atoms: #: $-x+1$, $y$, $-z+\frac{1}{2}$.

In this intricate structure, the $Cu^I$ ion is placed between two scorpionates into a tetrahedral ($N_2S_2$) ligand environment. We observe the same key structural features as in the $Cu^I$ complex (K[**11**])$_2$ (Figure 6) of the monotopic scorpionate [**5**]$^-$ (mean values of the Cu–S bonds: 2.264(2) Å in (K[**11**])$_2$, 2.361(2) Å in **14**$(thf)_2$; mean values of the Cu–N bonds: 2.048(7) Å in (K[**11**])$_2$, 2.023(7) Å in **14**$(thf)_2$). The tris(pyrazol-1-yl)borate functionalities of the two ligands bind jointly to the potassium ion K(2) with bond lengths of 2.840(8) Å. Additional short contacts are established between K(2) and the sulfur atoms (K(2)–S(1) = 3.385(3) Å) as well as the phenylene rings (K(2)–COG($C_6H_4$) = 3.051 Å; COG = ring centroid). Two more potassium ions, K(1) and the symmetry-related K(1#), coordinate to the metallomacrocyclic core to maintain charge neutrality. K(1) binds to one THF molecule, one pyrazolyl ring of a heteroscorpionate fragment, one pyrazolyl ring of the corresponding homoscorpionate moiety, and to the phenylene spacer. Each repeat unit is connected to the neighboring unit through pz(N(41)) and pz(N(51)), which bind to K(1*) (*: $-x+\frac{3}{2}$, $-y+\frac{3}{2}$, $-z+1$) in a σ- and π-mode, respectively. Interestingly, a striking similarity is obvious between the coordination spheres of K(1)/K(2) in the potassium salt $K_2$[**10**]$(thf)_2$ and in the $Cu^I$ complex **14**$(thf)_2$.

**Electrochemical investigations**: Compounds K[**5**], K[**11**], and **12** were investigated by cyclic voltammetry ($CH_2Cl_2$, $[NBu_4][B(C_6F_5)_4]$ (0.05 M), versus FcH/$FcH^+$; see the Supporting Information for cyclic voltammograms of K[**5**] in Figure 2aS and K[**11**] in Figure 2bS). The $K^+$ salt of the free ligand (K[**5**]) is electrochemically inactive in the potential range between 0.75 V and −1.75 V; in the more anodic regime, an irreversible oxidation process takes place.

In the potential range between 1.30 V and −2.10 V, the cyclic voltammogram (CV) of the $Cu^I$ complex K[**11**] shows three irreversible redox events with peak potentials of $E_{pa} \approx -0.71$ V, 0.27 V, and $E_{pc} \approx -1.49$ V.

$Cu^{II}$ complex **12** reveals two irreversible redox events at $E_{pa} \approx -0.79$ V and $E_{pc} \approx$ -1.65 V (Figure 10). In more oxidizing conditions, **12** undergoes a further irreversible transition

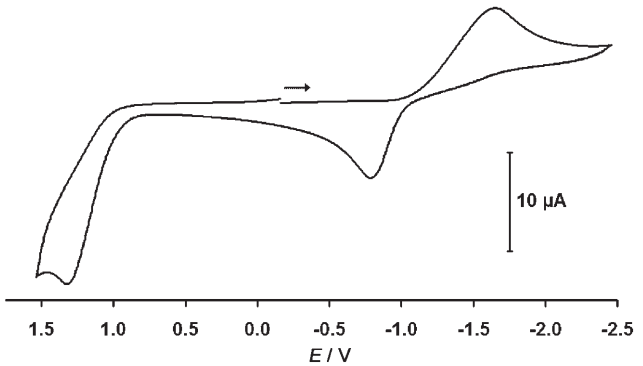


Figure 10. Cyclic voltammogram of **12** vs. FcH/$FcH^+$; $CH_2Cl_2$, $[NBu_4][B(C_6F_5)_4]$ as supporting electrolyte (0.05 M), scan rate 200 $mVs^{-1}$.

that is also observed in the CV of K[**5**] and therefore attributed to a ligand-centered process.

The determination of peak potentials of K[**11**] is associated with estimated error margins of ± 0.05 V. Moreover, $E_{pc}$ and $E_{pa}$ of **12** were found to be somewhat concentration dependent. Given this background, we attribute the redox

  

waves $E_{pa} \approx -0.71$ V/$E_{pc} \approx -1.49$ V (CV of the $Cu^{I}$ complex) and $E_{pa} \approx -0.79$ V/$E_{pc} \approx -1.65$ V (CV of the $Cu^{II}$ complex) to the same electron transfer reaction, which in both samples occurs between the species $[NBu_4]^+[\mathbf{11}]^- \rightleftarrows \mathbf{12}$. The highly cathodic value of $E_{pc}$ is likely owed to the fact that the $Cu^{II}$ ion is coordinated by two negatively charged ligands. Moreover, provided that the molecular structure of **12** in solution resembles its solid state structure, a square-pyramidal ($N_4S$) donor set is not well-suited to stabilize the $Cu^{I}$ state. It is therefore plausible that the initially created species undergoes ligand rearrangement to form a tetrahedral $Cu^{I}$ complex. As a consequence, the redox event becomes electrochemically irreversible. The associated return peak corresponds to the transformation of the tetrahedral $Cu^{I}$ complex into the corresponding $Cu^{II}$ compound that subsequently relaxes to the original structure.

The electrochemical properties of our complex stand in stark contrast to a related system in which the copper ion is surrounded by two chelating 1-methyl-2-((methylthio)-methyl)-1*H*-benzimidazole (mmb) ligands. $[Cu(mmb)_2][BF_4]$ undergoes an electrochemically reversible oxidation at 0.31 V vs. $FcH/FcH^+$.[65] In accordance with that is the apparent similarity between the molecular structures of $[Cu^{I}(mmb)_2]^+$ and $[Cu^{II}(mmb)_2(\eta^1\text{-}OClO_3)]^+$ as it has been confirmed by X-ray crystallography for the solid state and by DFT calculations for the gas phase.[65]

The redox event at $E_{pa} \approx 0.27$ V in the voltammogram of K[**11**] was not detected in the CV of **12**. We suggest as an explanation that a cation exchange equilibrium leads to the coexistence of K[**11**] and $[NBu_4]^+[\mathbf{11}]^-$ and that these two species have different oxidation potentials, i.e., 0.27 V and −0.71 V, respectively. The more anodic redox potential of K[**11**] with respect to $[NBu_4]^+[\mathbf{11}]^-$ can then be rationalized by assuming that the former exists as contact ion pairs in $CH_2Cl_2$ solution, whereas less tightly associated ions are present in solutions of the latter. We note in this context that the $Cu^{I}/Cu^{II}$ redox couple covers a broad range of standard oxidation potentials (exceeding variations of 1 V) depending on the particular ligand environment, the solvent, and on the nature of the counter ions (see p. 418 of ref. [51b]).

**Quantum chemical calculations**: Density functional theory (DFT) at the BP86 level including the COSMO continuum model (solvent $CH_2Cl_2$) was employed in order to scrutinize the hypothesis that a transition from the contact ion pair K[**11**] to the largely solvent separated system $[NBu_4]^+[\mathbf{11}]^-$ can indeed cause a shift in the corresponding $Cu^{I}/Cu^{II}$ redox potential of almost 1 V. Furthermore, we provide a theoretical assessment of the surprisingly cathodic potential required for the reduction of **12**. Details of the theoretical strategies are given in the section Experimental and Computational Methods below.

As one cannot necessarily expect the solid-state structures of $[\mathbf{11}]^-$ and **12** to prevail in solution, we also considered a selected number of reasonable structural isomers. $Cu^{I}$ ions are known to possess a high affinity both to nitrogen- and to sulfur-donor ligands.[66] We have, therefore, included the three tetrahedral species $[Cu^{I}(N_4)^{tet}]^-$, $[Cu^{I}(N_3S)^{tet}]^-$, and $[Cu^{I}(N_2S_2)^{tet}]^-$ into our DFT study (Figure 11). $Cu^{II}$ ions, in turn, have a significantly greater tendency to bind to amine

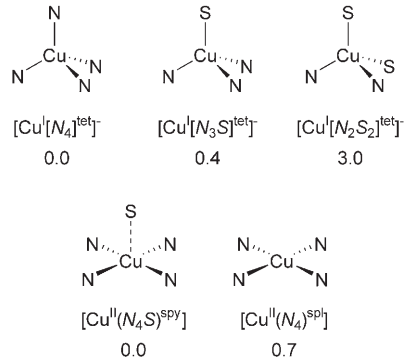


Figure 11. Relative energies ($\Delta E$ in kcal mol$^{-1}$ obtained at the BP86/SDD(Cu)TZVP(+COSMO:$CH_2Cl_2$)//BP86/SDD(Cu)TZVP level) between different coordination polyhedra of $[\mathbf{11}]^-$ (top row) and **12** (bottom row).

than to thioether ligands.[66] Our calculations on the $Cu^{II}$ complex **12** were therefore restricted to the two most plausible isomers, the square-pyramidal structure $[Cu^{II}(N_4S)^{spy}]$ (see the X-ray crystal structure analysis) and its square-planar congener $[Cu^{II}(N_4)^{spl}]$ (Figure 11). Calculated relative energies ($\Delta E$ in kcal mol$^{-1}$) with respect to the most stable isomer are compiled in Figure 11.

First we note a pleasing agreement between the experimentally determined bond lengths and angles of K[**11**] and **12** with the corresponding calculated values for $K[Cu^{I}(N_2S_2)^{tet}]$ and $[Cu^{II}(N_4S)^{spy}]$, respectively (see the Supporting Information).

The $Cu^{I}$ complex $[Cu^{I}(N_4)^{tet}]^-$ represents the most stable structure of all three anionic isomers. The $[Cu^{I}(N_3S)^{tet}]^-$ isomer is slightly less stable ($\Delta E = 0.4$ kcal mol$^{-1}$). Replacement of a second pyrazolyl ligand by a (methylthio)methyl group leads to a further increase in energy by 2.6 kcal mol$^{-1}$ ($[Cu^{I}(N_2S_2)^{tet}]^-$), even though one might have anticipated the $Cu^{I}$ ion to bind preferably to the softer (methylthio)-methyl donors. At this point we note, however, that the energy differences obtained here might fall within the typical error margins of the method employed,[67] and thus we refrain from providing any definitive statement with regard to the most stable coordination isomer of the free anion. We would rather see these results as an indication for the presence of a set of flexible isomers of $[\mathbf{11}]^-$ in solution, which is in accord with the NMR spectroscopic results on K[**11**] (see above). In the crystal lattice, we observed the seemingly least stable $[Cu^{I}(N_2S_2)^{tet}]^-$ coordination mode for the complex anion of K[**11**]. A closer inspection of the solid state structure suggests, however, a counterion effect as the likely explanation, because the $K^+$ cation in crystalline K[**11**] is π-coordinated to two pyrazolyl rings,[30,31,47,68] one from each scorpionate ligand. Such a type of molecular pocket is only

  

available in the $[Cu^{I}(N_2S_2)^{tet}]^-$ polyhedron but in none of the others. The $(N_2S_2)$ ligand environment therefore appears to be stabilized through π-coordination of the potassium counter ion (the structure of this contact ion pair was indeed shown to correspond to a minimum on the potential energy surface). It should be emphasized that π-interactions between $K^+$ and $[\mathbf{11}]^-$ may also be relevant in the liquid phase as they can lead to different distributions of coordination polyhedra in solutions of K[**11**] as compared to samples of $[\mathbf{11}]^-$ generated by reduction of $Cu^{II}$-complex **12** under the conditions of a CV experiment (i.e. in solutions containing non-coordinating $[NBu_4]^+$-salts as supporting electrolytes).

The crystal structure of **12** reveals a square-pyramidal complex with a long axial Cu–S bond of 2.805(3) Å suggesting a weakly coordinated (methylthio)methyl ligand. A very similar five-coordinated structure was found to be a minimum on the potential energy surface of **12** by reoptimization of the crystallographically determined structural parameters ($[Cu^{II}(N_4S)^{spy}]$; Figure 11). Avoiding of the Cu–S contact by turning the $CH_2SMe$ arm by 90° about the B–C bond and subsequent reoptimization of the structure results in an energy increase of merely 0.7 kcal mol$^{-1}$ for the resulting square-planar (spl) species $[Cu^{II}(N_4)^{spl}]$.

All in all, our calculations lead to the conclusion that the tetrahedral $Cu^{I}$ complex $[Cu^{I}(N_4)^{tet}]^-$ and the square-planar $Cu^{II}$ complex $[Cu^{II}(N_4)^{spl}]$ should be among the most abundant isomers in solutions of $[\mathbf{11}]^-$ and **12**, respectively. With regard to the interconversion of both species under electrochemical conditions it is important to note that $[Cu^{I}(N_4)^{tet}]^-$ cannot simply rearrange into $[Cu^{II}(N_4)^{spl}]$ by counterrotation of the two N–Cu–N planes. This reorganization is blocked by the pyrazolyl protons in the 3-positions of the scorpionate ligands (Figure 3S in the Supporting Information). Indeed, we located a second minimum resulting from geometry optimization commencing at the tetrahedral $Cu^{I}$ coordination environment, from which the ligands arrange as closely as possible into the square planar geometry after oxidation to the $Cu^{II}$ state. The resulting distorted square planar (dspl) isomer $[Cu^{II}(N_4)^{dspl}]$ is less stable than $[Cu^{II}(N_4S)^{spy}]$ by 3.1 kcal mol$^{-1}$.

With this picture at hand, we can now turn to the electron transitions and structural rearrangements taking place during the cyclic voltammetric measurements on K[**11**] and **12**. An important aspect of most microscopic theories of electron transfer is the assumption that the reactants and products share a common nuclear configuration at the moment of the actual act of oxidation or reduction.[69] We thus see the experimental peak potentials arising as a consequence of vertical oxidation or reduction events. Accordingly, we simulate these processes by computing the vertical ionization potentials (IE) or electron affinities of the respective species. We relate the computed potentials to that obtained for the ferrocene/ferrocenium ($FcH/FcH^+$) redox couple (computed: $IE_{FcH}=119.2$ kcal mol$^{-1}$), which serves as internal standard also in our CV measurements. Computed energy differences (obtained in kcal mol$^{-1}$) were converted into electrochemical potentials by division by the Faraday constant $F$ (403305.5 C cal$^{-1}$).

The cyclic voltammogram of K[**11**] is considered first (Scheme 4). In the initial step, vertical ionization of $K[Cu^{I}(N_2S_2)^{tet}]$ takes place, leading to the isostructural $Cu^{II}$ complex $[K\{Cu^{II}(N_2S_2)^{tet}\}]^+$. This process is computed to require an electrode potential of 0.31 V, which compares well with the experimental peak potential of $E_{pa}=0.27$ V.

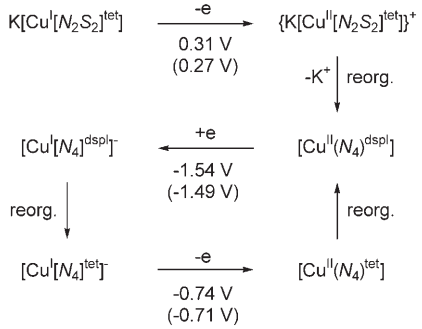


Scheme 4. Proposed pathways for reactions taking place during electrochemical conversion of K[**11**]. Experimental data (in brackets) were taken from the cyclic voltammogram of K[**11**]; notation of coordination polyhedra: see Figure 11 and text for details.

After the electron transfer, the $K^+$ ion dissociates from the $Cu^{II}$ complex and the ligand sphere of $[Cu^{II}(N_2S_2)^{tet}]$ reorganizes to give the distorted square-planar (dspl) isomer $[Cu^{II}(N_4)^{dspl}]$. Subsequent vertical reduction of $[Cu^{II}(N_4)^{dspl}]$ yields the corresponding $Cu^{I}$ complex $[Cu^{I}(N_4)^{dspl}]^-$. The calculated potential required for this transition amounts to −1.54 V, in good agreement with the experimental peak potential of $E_{pc}=-1.49$ V taken from the CV of K[**11**]. In contrast, vertical reduction of the *undistorted* isomer $[Cu^{II}(N_4)^{spl}]$ would correspond to a highly cathodic potential value of −2.23 V, a clear indication that the *distorted* square planar $Cu^{II}$ complex is responsible for the redox wave at $E_{pc}=-1.49$ V in the cyclic voltammogram of K[**11**] (cf. the concept of the "entatic state" of enzyme active sites[70]). $[Cu^{I}(N_4)^{dspl}]^-$ rearranges to the more stable tetrahedral structure $[Cu^{I}(N_4)^{tet}]^-$. Oxidation of this free anion to the neutral complex $[Cu^{II}(N_4)^{tet}]$ takes place at a substantially more negative potential (-0.74 V) than the oxidation of the contact ion pair K[**11**] (0.31 V). The value of −0.74 V compares well with the experimentally determined peak potential $E_{pa}=-0.71$ V for K[**11**]. Oxidation of $[Cu^{I}(N_2S_2)^{tet}]^-$ to $[Cu^{II}(N_2S_2)^{tet}]$ is computed to occur at −0.32 V, which is in contrast to the experimental finding and therefore again suggests that $[Cu^{I}(N_4)^{tet}]^-$ is indeed the most stable coordination geometry for the free ion, whereas the solid state isomer $[Cu^{I}(N_2S_2)^{tet}]^-$ is clearly negligible in solution.

As expected and outlined above, the two redox transitions visible in the CV of the $Cu^{II}$ complex **12** are also observed in the CV of K[**11**], which indicates that in both cases the same species are involved in the electron transfer processes. Following our quantum chemical interpretation, this points

  

to the predominance of the distorted square-planar configuration [$Cu^{II}(N_4)^{dspl}$] in both experiments. Yet, in the case of **12**, this is somewhat counterintuitive considering the fact that we have prepared the sample by dissolving single crystals evidently containing the undistorted square-planar isomer [$Cu^{II}(N_4)^{spl}$]. For this species, however, a redox potential of −2.23 V results from our DFT calculations, as opposed to a value of −1.54 V for [$Cu^{II}(N_4)^{dspl}$] and in disagreement with the experimental redox potentials of −1.49 V and −1.65 V for K[**11**] and **12**, respectively.

At first sight, one could plainly see this as a large error in the DFT description of the intricate electronic processes behind CV measurements. Notwithstanding all appropriate skepticism as to the uncritical use of DFT for chemical problems involving transition metal complexes,[71] we did not find any hint for a source of error in the quantum chemical results. And indeed, given the overall good performance of the DFT description of CV data above, this would appear as an unexpected failure of DFT for an otherwise innocuous species that largely resembles all other isomers studied here. Also, we have previously established the level of DFT employed here as a very robust means to predict trends in the electrochemical properties of a homologous series of transition metal complexes.[72] Rather than plainly assuming a fundamental DFT error, we suggest the following chemical scenario as an alternative explanation: Assuming a fast equilibrium between the *distorted* and the *undistorted* isomers [$Cu^{II}(N_4)^{dspl}$] and [$Cu^{II}(N_4)^{spl}$] any amount of [$Cu^{II}(N_4)^{dspl}$] present will give rise to a reduction wave at about −1.5 V in the course of the CV scan. Simultaneously, the [$Cu^{II}(N_4)^{dspl}$] consumed in this process will be replenished from the reservoir of the undistorted isomer [$Cu^{II}(N_4)^{spl}$]. Provided that the scan rate is slow on the time scale of the equilibrium, no undistorted [$Cu^{II}(N_4)^{spl}$] will be left to yield a signal at the predicted redox potential of −2.23 V.

## Conclusion

Straightforward protocols have been elaborated for preparing the ($N_2S$) scorpionate ligand [$PhBpz_2(CH_2SMe)$]$^-$ ([**5**]$^-$) and the *hetero*ditopic poly(pyrazol-1-yl)borate *p*-[$pz_3B$–$C_6H_4$–$Bpz_2(CH_2SMe)$]$^{2-}$ ([**10**]$^{2-}$). In our hands, the key to success was the use of TMEDA-free $LiCH_2SMe$ for the introduction of the sulfur donor group. With regard to the synthesis of [**10**]$^{2-}$ it was important to recognize that the intermediate [(methylthio)methyl]borane *p*-$Me_3Si$-$C_6H_4$-B(Br)($CH_2SMe$) forms dimeric B–S adducts in solution. As a result, the sulfur atom is protected from further electrophilic attack so that $BBr_3$ can be employed in a subsequent silicon-boron exchange step leading to the unsymmetric building block *p*-$Br_2B$–$C_6H_4$-B(Br)($CH_2SMe$).

(Hetero)ditopic ligands are important for the preparation of (hetero)dinuclear complexes in which an interaction between the two metal sites brings about chemical and/or physical properties not exhibited by the mononuclear constituents alone. The discorpionate [**10**]$^{2-}$ is designed to mimic the two ligation sites of the copper enzymes peptidylglycine α-hydroxylating monooxygenase and dopamine β-monooxygenase in which the cooperative action of one [$his_3Cu$] and one [$his_2$(met)Cu] fragment leads to oxidative C–H activation (his = histidine; met = methionine). In a systematic study, we first investigated the coordination properties of the monotopic tripod [**5**]$^-$ toward $Cu^I$ and $Cu^{II}$ ions and isolated 2:1 complexes K[$Cu^I$(**5**)$_2$] (K[**11**]) and [$Cu^{II}$(**5**)$_2$] (**12**). The solid state structure of K[**11**] revealed a tetrahedral ($N_2S_2$) coordination environment for the $Cu^I$ ion, whereas the $Cu^{II}$ ion of **12** possesses a square-pyramidal ($N_4S$) ligand sphere. In the cyclic voltammograms of K[**11**] and **12**, the $Cu^I$/$Cu^{II}$ transition is irreversible, most likely because electron transfer is accompanied by extensive ligand reorganization. The quantum chemical assessment of the redox processes provided detailed insights into the underlying elementary processes and the nature of the dominant species involved.

After K[**11**] had been treated with dry air, $Cu^{II}$ complex **12** was isolated as the main product together with smaller amounts of a decomposition product indicating oxidative B–C activation. So far, we have no evidence for sulfur oxidation.

Addition of excess CuCl to $K_2$[**10**] led to the formation of a compound $K_3$[Cu(**10**)$_2$] (**14**), which again contains two ligand molecules per $Cu^I$ center. The $Cu^I$ ion binds to both heteroscorpionate moieties and thereby establishes a coordination environment similar to that of the $Cu^I$ ion in K[**11**].

By using the same synthetic approach as for [**5**]$^-$ and [**10**]$^{2-}$, an attractive goal for future ligand development lies in the preparation of more sterically demanding derivatives that are able to form well-defined complexes featuring only one scorpionate unit per copper ion. Such complexes are not only expected to show an increased affinity toward elemental oxygen but also to kinetically stabilize the primary intermediates of the $O_2$-activation sequence so that they can be unambiguously identified.[73–77]

## Experimental and Computational Methods

**General remarks**: All reactions were carried out under a nitrogen atmosphere using Schlenk tube techniques. Reaction solvents were freshly distilled under argon from Na/Pb alloy (pentane, hexane) and Na/benzophenone ($C_6H_6$, toluene, $Et_2O$, THF) prior to use; $C_6D_6$ was distilled under nitrogen from Na/benzophenone and stored in a Schlenk flask. NMR: Bruker AM 250, Avance 300, Avance 400, and DPX 250. Chemical shifts are referenced to residual solvent signals ($^1H$, $^{13}C\{^1H\}$) or external $BF_3$·$Et_2O$ ($^{11}B\{^1H\}$). Abbreviations: s = singlet, d = doublet, vtr = virtual triplet, m = multiplet, br = broad, n.o. = signal not observed, Ph = phenyl, Ar = *p*-phenylene, pz = pyrazolyl ring of a bis(pyrazol-1-yl)borate unit, pz′ = pyrazolyl ring of a tris(pyrazol-1-yl)borate unit. $BBr_3$ was stored over mercury under a nitrogen atmosphere. $SMe_2$ and $BBr_3$ are commercially available. $PhBBr_2$,[42,45] *p*-$Me_3Si$-$C_6H_4$-$BBr_2$,[44,45] and $LiCH_2SMe$[43] were synthesized following literature procedures.

***Caution!*** *$SMe_2$ is a flammable liquid of pungent odor; donor-free $LiCH_2SMe$ violently explodes upon exposure to air or upon thermolysis under an argon atmosphere.*[43]

**Synthesis of 2**: $C_6H_6$ (30 mL) was added to neat $LiCH_2SMe$ (0.48 g; 7.05 mmol) and the resulting suspension cooled to 6 °C. A solution of

  

$PhBBr_2$ (1.75 g; 7.05 mmol) in $C_6H_6$ (8 mL) was added dropwise with stirring over a period of 45 min. The reaction mixture was allowed to warm to RT and stirred for 12 h. The resulting colorless suspension was filtered and the filtrate evaporated to dryness in vacuo. Recrystallization by slow diffusion of pentane into a solution of the crude product in $C_6H_6$ gave colorless crystals of **2**. Yield: 1.36 g (2.97 mmol, 84%). $^1$H NMR (400.1 MHz, $C_6D_6$): $\delta = 7.89$ (d, 4H; PhH-*o*), 7.29 (vtr, 4H; PhH-*m*), 7.19 (t, 2H; PhH-*p*), 2.64, 2.08 (2×d, $^2J$(H,H) = 12.7 Hz, 2×2H; $BCH_2$), 1.36 ppm (s, 6H; SMe); $^{13}$C NMR (100.6 MHz, $C_6D_6$): $\delta = 133.3$ (PhC-*o*), 128.3 (PhC-*p*), 128.3 (PhC-*m*), 34.9 (br, $BCH_2$), 20.3 ppm (SMe), n.o. (PhC-*i*); $^{11}$B NMR (128.4 MHz, $C_6D_6$): $\delta = 2.5$ ppm ($h_{1/2} = 250$ Hz); elemental analysis calcd (%) for $C_{16}H_{20}B_2Br_2S_2$ [457.88]: C 42.14, H 4.48; found: C 41.97, H 4.40.

**Synthesis of 3**: $C_6H_6$ (25 mL) was added to neat $LiCH_2SMe$ (0.57 g; 8.37 mmol) and the resulting suspension cooled to 6°C. A solution of $PhBBr_2$ (1.04 g; 4.20 mmol) in $C_6H_6$ (15 mL) was added dropwise with stirring over a period of 40 min. The reaction mixture was allowed to warm to RT and stirred for 12 h. The resulting colorless suspension was filtered and the filtrate concentrated in vacuo until a colorless microcrystalline precipitate formed. Pentane (40 mL) was added, the insoluble product was collected on a frit and dried in vacuo. The crude product was not analytically pure, but its purity was sufficiently high for further transformation into $[PhBpz(CH_2SMe)_2]^-$.[18] Yield of the crude material: approx. 65%; single crystals of **3** formed from an NMR sample ($C_6D_6$) at RT. Yield of single crystalline material: 0.08 g (0.19 mmol, 9%). To facilitate its NMR-spectroscopic characterization, **3** was transformed into the pyridine adduct $PhB(CH_2SMe)_2$·py. $^1$H NMR (400.1 MHz, $C_6D_6$): $\delta = 8.50$ (d, 2H; pyH-*o*), 7.51 (d, 2H; PhH-*o*), 7.37 (vtr, 2H; PhH-*m*), 7.25 (t, 1H; PhH-*p*), 6.70–6.63 (m, 1H; pyH-*p*), 6.35 (vtr, 2H; pyH-*m*), 2.55, 2.44 (2×d, $^2J$(H,H) = 11.9 Hz, 2×2H; $BCH_2$), 2.02 ppm (s, 6H; SMe); $^{13}$C NMR (100.6 MHz, $C_6D_6$): $\delta = 146.9$ (pyC-*o*), 139.4 (pyC-*p*), 133.0 (PhC-*o*), 127.7 (PhC-*m*), 126.0 (PhC-*p*), 124.3 (pyC-*m*), 33.7 (br, $BCH_2$), 19.9 ppm (SMe), n.o. (PhC-*i*); $^{11}$B NMR (128.4 MHz, $C_6D_6$): $\delta = 0.0$ ppm ($h_{1/2} = 160$ Hz).

**Synthesis of 4**: **2** (0.34 g; 0.74 mmol) was dissolved in $C_6H_6$ (20 mL) and the solution cooled to 6°C. Neat $Me_2NSiMe_3$ (0.25 mL; 0.19 g; 1.62 mmol) was added through a syringe, the resulting colorless suspension was allowed to warm to RT and stirred for 12 h. All volatiles were removed in vacuo leaving behind the product as a colorless waxy solid. Yield: 0.24 g (1.23 mmol, 83%). $^1$H NMR (400.1 MHz, $C_6D_6$): $\delta = 7.52$ (d, 2H; PhH-*o*), 7.28 (vtr, 2H; PhH-*m*), 7.20 (t, 1H; PhH-*p*), 2.64, 2.47 (2×s, 2×3H; NMe), 2.22 (s, 2H; $BCH_2$), 1.88 ppm (s, 3H; SMe); $^{13}$C NMR (100.6 MHz, $C_6D_6$): $\delta = 132.0$ (PhC-*o*), 127.9, 127.9 (PhC-*m*,*p*), 41.0, 39.7 (NMe), 24.4 (br, $BCH_2$), 19.1 ppm (SMe), n.o. (PhC-*i*); $^{11}$B NMR (128.4 MHz, $C_6D_6$): $\delta = 40.6$ ppm ($h_{1/2} = 150$ Hz).

**Synthesis of Li[5]**: **4** (0.58 g; 3.02 mmol) was dissolved in toluene (20 mL). To the stirred solution was added a solid mixture of Hpz (0.21 g; 3.08 mmol) and Lipz (0.22 g; 2.95 mmol). The resulting suspension was heated to reflux for 12 h. Evaporation of the pale yellow solution in vacuo yielded a colorless solid foam. Recrystallization by gas diffusion of pentane into a toluene solution of the crude product yielded colorless crystals of $(Li[\mathbf{5}])_2$. Yield: 0.79 g (2.71 mmol, 92%). $^1$H NMR (250.1 MHz, [D$_8$]THF): $\delta = 8.18$, 7.45 (2×d, 2×2H; pzH-3,5), 6.93–6.84, 6.47–6.37 (2×m, 3H, 2H; PhH), 6.14 (vtr, 2H; pzH-4), 2.30 (s, 2H; $BCH_2$), 2.06 ppm (s, 3H; SMe); $^{13}$C NMR (62.9 MHz, [D$_8$]THF): $\delta =$ 139.3, 135.8 (pzC-3,5), 132.2, 126.9 (PhC), 125.1 (PhC-*p*), 102.9 (pzC-4), 33.6 (br, $BCH_2$), 20.1 ppm (SMe), n.o. (PhC-*i*); $^{11}$B NMR (80.3 MHz, [D$_8$]THF): $\delta = -0.8$ ($h_{1/2} = 125$ Hz); elemental analysis calcd (%) for $C_{14}H_{16}BLiN_4S$ [290.12]·0.25 $C_7H_8$ [92.14]: C 60.41, H 5.79, N 17.89; found: C 59.85, H 6.42, N 17.19. Note: The presence of 0.25 equiv of toluene in the bulk material was proven by $^1$H NMR spectroscopy.

**Synthesis of K[5]**: **4** (0.14 g; 0.72 mmol) was dissolved in toluene (6 mL). To the stirred solution was added a solid mixture of Hpz (0.05 g; 0.73 mmol) and Kpz (0.08 g; 0.75 mmol). The resulting suspension was heated to reflux for 3 h, cooled to RT and stirred for 12 h. The product was isolated by filtration as a colorless microcrystalline solid. Colorless single crystals of K [**5**] were obtained by slow diffusion of $Et_2O$ into its THF solution. Yield: 0.20 g (0.62 mmol, 86%). $^1$H NMR (300.0 MHz, [D$_8$]THF): $\delta = 7.87$, 7.26 (2×d, 2×2H; pzH-3,5), 7.04–6.92, 6.90–6.84 (2×m, 3H, 2H; PhH), 5.99 (vtr, 2H; pzH-4), 2.40 (s, 2H; $BCH_2$), 1.94 ppm (s, 3H; SMe); $^{13}$C NMR (62.9 MHz, [D$_8$]THF): $\delta = 138.3$ (pzC-3 or 5), 134.1 (PhC), 133.7 (pzC-3 or 5), 126.7 (PhC), 125.1 (PhC-*p*), 102.6 (pzC-4), 33.8 (br, $BCH_2$), 20.1 ppm (SMe), n.o. (PhC-*i*); $^{11}$B NMR (96.3 MHz, [D$_8$]THF): $\delta = -1.0$ ppm ($h_{1/2} = 110$ Hz); elemental analysis calcd (%) for $C_{14}H_{16}BKN_4S$ [322.28]·0.5 $H_2O$ [18.01] : C 50.75, H 5.17, N 16.90; found: C 50.77, H 4.99, N 16.57. Note: K[**5**] is hygroscopic.

**Synthesis of 6**: *p*-$Me_3Si$-$C_6H_4$-$SiMe_3$ (0.99 g; 4.45 mmol) was dissolved in $C_6H_6$ (10 mL). Neat $BBr_3$ (1.11 g; 4.43 mmol) was added through a syringe and the pale yellow solution stirred for 18 h. All volatiles were removed in vacuo leaving behind the product as a yellow oil. Yield: 1.41 g (4.40 mmol, 99%). $^1$H NMR (400.1 MHz, $C_6D_6$): $\delta = 8.10$, 7.34 (2×d, $^3J$(H,H) = 8.0 Hz, 2×2H; ArH), 0.14 ppm (s, 9H; SiMe); $^{13}$C NMR (100.6 MHz, $C_6D_6$): $\delta = 150.1$ (*C*Si), 136.8, 133.3 (ArC), −1.6 ppm (SiMe), n.o. (*C*B); $^{11}$B NMR (128.4 MHz, $C_6D_6$): $\delta = 57.5$ ppm ($h_{1/2} = 285$ Hz).

**Synthesis of 7**: $C_6H_6$ (15 mL) was added to solvent-free $LiCH_2SMe$ (0.52 g; 7.64 mmol) and the resulting suspension cooled to 6°C. A solution of **6** (2.53 g; 7.91 mmol) in $C_6H_6$ (10 mL) was added dropwise with stirring over a period of 30 min. The reaction mixture was allowed to warm to RT and stirred for 12 h. The resulting pearl white suspension was filtered and the filtrate evaporated to dryness in vacuo leaving behind the product as a colorless white solid. Yield: 1.83 g (3.04 mmol, 80%). Single crystals were grown by gas-phase diffusion of hexane into a benzene solution of **7**. $^1$H NMR (400.1 MHz, $C_6D_6$): $\delta = 7.94$, 7.59 (2×d, $^3J$(H,H) = 8.1 Hz, 2×4H; ArH), 2.73, 2.18 (2×d, $^2J$(H,H) = 12.7 Hz, 2×2H; $BCH_2$), 1.40 (s, 6H; SMe), 0.27 ppm (s, 18H; SiMe); $^{13}$C NMR (100.6 MHz, $C_6D_6$): $\delta = 140.0$ (*C*Si), 133.4, 132.8 (ArC), 20.4 (SMe), −1.0 ppm (SiMe), n.o. (*C*B, $BCH_2$); $^{11}$B NMR (128.4 MHz, $C_6D_6$): $\delta =$ 3.0 ppm ($h_{1/2} = 585$ Hz); elemental analysis calcd (%) for $C_{22}H_{36}B_2Br_2S_2Si_2$ [602.25]: C 43.87, H 6.03; found: C 43.62, H 5.96.

**Synthesis of 8**: **7** (2.10 g; 3.49 mmol) was dissolved in $C_6H_6$ (50 mL). Neat $BBr_3$ (1.75 g; 6.98 mmol) was added through a syringe and the colorless solution stirred for 18 h, whereupon a colorless precipitate formed which was collected on a frit. The crude product was washed with $C_6H_6$ (10 mL) and dried in vacuo. Yield: 1.33 g (1.67 mmol, 48%). $^1$H NMR (400.1 MHz, [D$_8$]toluene): $\delta = 8.16$, 7.74 (2×d, $^3J$(H,H) = 8.2 Hz, 2×4H; ArH), 2.52, 1.97 (2×d, $^2J$(H,H) = 12.5 Hz, 2×2H; $BCH_2$), 1.35 ppm (s, 6H; SMe); $^{13}$C NMR (100.6 MHz, [D$_8$]toluene): $\delta = 137.5$, 132.9 (ArC), 34 (very br, $BCH_2$), 20.3 ppm (SMe), n.o. (2×*C*B); $^{11}$B NMR (128.4 MHz, [D$_8$]toluene): $\delta = 2.2$ ppm (B(Br)($CH_2SMe$)), n.o. ($BBr_2$).

**Synthesis of 9**: **8** (1.15 g; 1.44 mmol) was suspended in $C_6H_6$ (40 mL). Neat $Me_2NSiMe_3$ (1.04 g; 8.87 mmol) was added through a syringe and the resulting pale pink solution stirred for 12 h. All volatiles were removed in vacuo to give the product as a pale yellow oil. Yield: 0.81 g (2.78 mmol, 97%). $^1$H NMR (250.1 MHz, $C_6D_6$): $\delta = 7.68$–7.56 (m, 4H; ArH), 2.69 (s, 3H; B(N*Me*$_2$)($CH_2SMe$)), 2.64 (s, 12H; B(N*Me*$_2$)$_2$), 2.57 (s, 3H; B(N*Me*$_2$)($CH_2SMe$)), 2.29 (s, 2H; $BCH_2$), 1.90 ppm (s, 3H; SMe); $^{13}$C NMR (62.9 MHz, $C_6D_6$): $\delta = 133.2$, 131.5 (ArC), 41.3 (B(N*Me*$_2$)$_2$), 41.2, 39.8 (B(N*Me*$_2$)($CH_2SMe$)), 19.2 ppm (SMe), n.o. (2×*C*B, $BCH_2$); $^{11}$B NMR (128.4 MHz, $C_6D_6$): $\delta = 40.7$ (1B, $h_{1/2} = 270$ Hz, B(N*Me*$_2$)-($CH_2SMe$)), 33.1 ppm (1B, $h_{1/2} = 190$ Hz, B(N*Me*$_2$)$_2$).

**Synthesis of $Li_2$[10]**: **9** (0.56 g; 1.92 mmol) was dissolved in toluene (30 mL). To the stirred solution was added a solid mixture of Hpz (0.39 g; 5.73 mmol) and Lipz (0.28 g; 3.80 mmol). The resulting suspension was heated to reflux for 11 h, cooled to RT and stirred for 1 h. The product was isolated by filtration as a pale cream-colored microcrystalline solid. Yield: 0.84 g (1.65 mmol, 86%). $^1$H NMR (400.1 MHz, [D$_8$]THF): $\delta = 8.00$ (d, 2H; pzH-3 or 5), 7.44 (d, 3H; pzH′-3 or 5), 7.42 (d, 2H; pzH-3 or 5), 7.00 (d, 3H; pzH′-3 or 5), 6.42–6.30 (m, 4H; ArH), 6.07 (vtr, 2H; pzH-4), 5.99 (vtr, 3H; pzH′-4), 2.26 (s, 2H; $BCH_2$), 2.03 ppm (s, 3H; SMe); $^{13}$C NMR (100.6 MHz, [D$_8$]THF): $\delta = 139.7$ (pzC′-3 or 5), 139.1 (pzC-3 or 5), 136.2 (pzC′-3 or 5), 135.7 (pzC-3 or 5), 132.3, 131.1 (ArC), 103.0 (pzC′-4), 102.6 (pzC-4), 34 (br, $BCH_2$), 20.0 ppm (SMe), n.o. (2×*C*B); $^{11}$B NMR (128.4 MHz, [D$_8$]THF): $\delta = 4.1$ ($h_{1/2} = 400$ Hz), 1.6 ppm ($h_{1/2} = 280$ Hz); elemental analysis calcd (%) for $C_{23}H_{24}B_2Li_2N_{10}S$ [508.07]·0.5 $H_2O$ [18.02]: C 53.42, H 4.87, N 27.08; found: C 53.32, H 4.98, N 27.32.

  

**Synthesis of $K_2$[10]**: **9** (0.81 g; 2.78 mmol) was dissolved in toluene (40 mL). To the stirred solution was added a solid mixture of Hpz (0.60 g; 8.81 mmol) and Kpz (0.59 g; 5.56 mmol). The resulting suspension was heated to reflux for 24 h. The product was isolated by filtration as a colorless microcrystalline solid. Colorless single crystals of $K_2$[**10**]-$(thf)_2$ were obtained by slow evaporation of a THF solution. Yield: 1.45 g (2.53 mmol, 91%). $^1$H NMR (300.0 MHz, [$D_8$]THF): $\delta = 7.57$ (d, 2H; pzH-3 or 5), 7.38 (d, 3H; pzH′-3 or 5), 7.23 (d, 2H; pzH-3 or 5), 7.16 (d, 3H; pzH′-3 or 5), 7.02–6.89 (m, 4H; ArH), 6.01 (m, 3H; pzH′-4), 5.96 (m, 2H; pzH-4), 2.50 (s, 2H; $BCH_2$), 1.98 ppm (s, 3H; SMe); $^{13}$C NMR (62.9 MHz, [$D_8$]THF): $\delta = 139.5$ (pzC′-3 or 5), 138.3 (pzC-3 or 5), 134.8 (pzC′-3 or 5), 133.6 (ArC), 133.0 (pzC-3 or 5; ArC), 103.3 (pzC′-4), 102.7 (pzC-4), 33 (very br, $BCH_2$), 19.9 ppm (SMe), n.o. ($2\times CB$); $^{11}$B NMR (96.3 MHz, [$D_8$]THF): $\delta = 3.8$ ($h_{1/2} = 470$ Hz), 1.5 ppm ($h_{1/2} = 420$ Hz); elemental analysis calcd (%) for $C_{23}H_{24}B_2K_2N_{10}S$ [572.39]: C 48.26, H 4.23, N 24.47; found: C 47.62, H 4.16, N 23.81.

**Synthesis of K[11]**: **K[5]** (0.15 g; 0.47 mmol) and CuCl (0.06 g; 0.61 mmol) were suspended in toluene (25 mL). The reaction mixture was stirred for 2 d at RT After centrifugation, the pale green supernatant was evaporated to dryness in vacuo to give a pale green solid. Colorless single crystals were obtained by slow diffusion of pentane into a $C_6H_6$ solution of K[**11**]. Yield: 0.08 g (0.06 mmol, 26%). $^1$H NMR (250.1 MHz, [$D_8$]THF, 50 °C): $\delta = 7.35$ (n.r., 4H; pzH-3 or 5), 7.03–6.90 (m, 10H, pzH-3 or 5; PhH-*m*,*p*), 6.71 (n.r., 4H; PhH-*o*), 6.04 (n.r., 4H; pzH-4), 2.54 (n.r., 4H; $BCH_2$), 2.11 ppm (s, 6H; SMe); $^{13}$C NMR (62.9 MHz, [$D_8$]THF, 50 °C): $\delta = 140.0$ (br, pzC-3 or 5), 135.7 (br, pzC-3 or 5), 133.0 (br, PhC-*o*), 127.4 (br, PhC-*m*), 125.9 (br, PhC-*p*), 103.6 (br, pzC-4), 34.0 (br, $BCH_2$), 22.8 ppm (SMe); $^{11}$B NMR (80.3 MHz, [$D_8$]THF, 50 °C): $\delta = -0.8$ ppm ($h_{1/2} = 200$ Hz); elemental analysis calcd (%) for $C_{28}H_{32}B_2CuKN_8S_2$ [669.01]•$C_6H_6$ [78.11]: C 54.66, H 5.13, N 14.99; found: C 54.50, H 5.13, N 14.91.

**Synthesis of 12**: **K[5]** (0.35 g; 1.09 mmol) and $CuBr_2$ (0.13 g; 0.58 mmol) were suspended in toluene (50 mL). The reaction mixture was stirred at RT for 4 d. After centrifugation, the emerald green supernatant was evaporated to dryness in vacuo to give a purple microcrystalline solid. Dark purple single crystals were obtained by slow diffusion of hexane into a toluene solution of **12**. Yield 0.20 g (0.32 mmol, 59%). UV/vis (toluene): $\lambda_{max}$ ($\varepsilon$) = 615 (70), 390 (550), 319 nm (shoulder; 750 $mol^{-1}\,dm^3\,cm^{-1}$); elemental analysis calcd (%) for $C_{28}H_{32}B_2CuN_8S_2$ [629.90] :C 53.39, H 5.12, N 17.79; found: C 53.31, H 5.15, N 17.78.

**Reaction of K[11] with $O_2$**: Compressed air (dried over $P_4O_{10}$) was bubbled through a colorless solution of K[**11**] (0.29 g; 0.22 mmol) in $C_6H_6$ (10 mL) at RT over a period of 8 h. From the green paramagnetic reaction mixture, crystals were grown of the $Cu^{II}$ complex **12** (major component) and the degradation product **13**. Few single crystals of **13** were isolated by crystal picking.

**Synthesis of 14**: $K_2$[**10**] (0.02 g; 0.03 mmol) and CuCl (0.01 g; 0.10 mmol) were suspended in THF (20 mL). The resulting reaction mixture was stirred at RT for 7 d. After centrifugation, the pale green supernatant was evaporated to dryness in vacuo to give a pale green solid. Few colorless single crystals of **14**$(thf)_2$ were obtained by slow evaporation of a THF solution.

**Crystal structure analyses**: Crystals of **2**, (Li[**5**])$_2$, K[**5**], $K_2$[**10**]$(thf)_2$, (K[**11**])$_2$, **12**, **13**, and **14**$(thf)_2$ were measured by means of a STOE IPDS-II diffractometer with graphite-monochromated $MoK_\alpha$ radiation. An empirical absorption correction with program PLATON[78] was performed for all structures. The structures were solved by direct methods[79] and refined with full-matrix least-squares on $F^2$ using the program SHELXL97.[80] Hydrogen atoms were placed on ideal positions and refined with fixed isotropic displacement parameters using a riding model. For K[**5**], the absolute structure has been determined: Flack *x*-parameter 0.2(1). $K_2$[**10**]$(thf)_2$ crystallizes together with one equivalent of non-coordinated THF; (K[**11**])$_2$ and **14**$(thf)_2$ crystallize together with two equivalents of non-coordinated benzene and THF, respectively. CCDC 675967 (**2**), 675968 (**3**), 675969 ((Li[**5**])$_2$), 675970 (K[**5**]), 677107 (**7**), 675971 ($K_2$[**10**]$(thf)_2$), 675972 ((K[**11**])$_2$), 675973 (**12**), 675974 (**13**), and 675975 (**14**$(thf)_2$) contain the supplementary crystallographic data for this paper. These data can be obtained free of charge from The Cambridge Crystallographic Data Centre via www.ccdc.cam.ac.uk/data_request/cif.

**Electrochemical measurements**: All measurements were performed by using an EG&G Princeton Applied Research 263 A potentiostat with a platinum disc working electrode. Carefully dried ($CaH_2$) and degassed $CH_2Cl_2$ was used as solvent and [$NBu_4$][$B(C_6F_5)_4$] as supporting electrolyte (0.05 M). All potential values are referenced against the $FcH/FcH^+$ couple.

**Quantum chemical calculations**: Quantum chemical calculations were carried out employing the program Turbomole 5.9.[81] The BP86 functional[82,83] was used in combination with the TZVP basis set of Ahlrichs et al.[84] for all atoms except Cu, for which we employed the relativistic 10-electron core potential/basis set combination developed by Dolg et al.[85] For improved efficiency we made use of the resolution of identity (RI) approximation[86–90] and the TZV-J coulomb fitting basis set was used (ecp-10-mdf-J for Cu). Subsequent single point energy calculations were performed using the COSMO continuum model[91] (solvent $CH_2Cl_2$, dielectric constant at room temperature $\varepsilon = 9.03$) to account for solvation effects.

## Acknowledgements

M.W. is grateful to the Deutsche Forschungsgemeinschaft (DFG) and the Fonds der Chemischen Industrie (FCI) for financial support. K.R. wishes to thank the Degussa Stiftung for a Ph.D. grant. Computer time provided by the CSC Frankfurt and the HLR Darmstadt is acknowledged.

[1] S. Trofimenko, *Chem. Rev.* **1993**, *93*, 943–980.
[2] S. Trofimenko, *Scorpionates - The Coordination Chemistry of Polypyrazolylborate Ligands*, Imperial College Press, London, **1999**.
[3] A. A. Barney, A. F. Heyduk, D. G. Nocera, *Chem. Commun.* **1999**, 2379–2380.
[4] J. C. Peters, J. D. Feldman, T. D. Tilley, *J. Am. Chem. Soc.* **1999**, *121*, 9871–9872.
[5] T. A. Betley, J. C. Peters, *Inorg. Chem.* **2003**, *42*, 5074–5084.
[6] M. Garner, J. Reglinski, I. Cassidy, M. D. Spicer, A. R. Kennedy, *Chem. Commun.* **1996**, 1975–1976.
[7] J. Reglinski, M. Garner, I. D. Cassidy, P. A. Slavin, M. D. Spicer, D. R. Armstrong, *J. Chem. Soc. Dalton Trans.* **1999**, 2119–2126.
[8] P. Ge, B. S. Haggerty, A. L. Rheingold, C. G. Riordan, *J. Am. Chem. Soc.* **1994**, *116*, 8406–8407.
[9] C. Ohrenberg, P. Ge, P. Schebler, C. G. Riordan, G. P. A. Yap, A. L. Rheingold, *Inorg. Chem.* **1996**, *35*, 749–754.
[10] C. Ohrenberg, C. G. Riordan, L. Liable-Sands, A. L. Rheingold, *Coord. Chem. Rev.* **1998**, *174*, 301–311.
[11] P. J. Schebler, C. G. Riordan, I. A. Guzei, A. L. Rheingold, *Inorg. Chem.* **1998**, *37*, 4754–4755.
[12] C. Ohrenberg, L. M. Liable-Sands, A. L. Rheingold, C. G. Riordan, *Inorg. Chem.* **2001**, *40*, 4276–4283.
[13] M. A. Casado, V. Hack, J. A. Camerano, M. A. Ciriano, C. Tejel, L. A. Oro, *Inorg. Chem.* **2005**, *44*, 9122–9124.
[14] J. A. Camerano, M. A. Casado, M. A. Ciriano, C. Tejel, L. A. Oro, *Chem. Eur. J.* **2008**, *14*, 1897–1905.
[15] C. M. Thomas, N. P. Mankad, J. C. Peters, *J. Am. Chem. Soc.* **2006**, *128*, 4956–4957.
[16] B. Benkmil, M. Ji, H. Vahrenkamp, *Inorg. Chem.* **2004**, *43*, 8212–8214.
[17] C. Kimblin, T. Hascall, G. Parkin, *Inorg. Chem.* **1997**, *36*, 5680–5681.
[18] S.-J. Chiou, P. Ge, C. G. Riordan, L. M. Liable-Sands, A. L. Rheingold, *Chem. Commun.* **1999**, 159–160.
[19] S.-J. Chiou, J. Innocent, C. G. Riordan, K.-C. Lam, L. Liable-Sands, A. L. Rheingold, *Inorg. Chem.* **2000**, *39*, 4347–4353.
[20] C. Kimblin, B. M. Bridgewater, T. Hascall, G. Parkin, *J. Chem. Soc. Dalton Trans.* **2000**, 1267–1274.

  

[21] C. Kimblin, B. M. Bridgewater, D. G. Churchill, T. Hascall, G. Parkin, *Inorg. Chem.* **2000**, *39*, 4240–4243.
[22] M. Shu, R. Walz, B. Wu, J. Seebacher, H. Vahrenkamp, *Eur. J. Inorg. Chem.* **2003**, 2502–2511.
[23] U. Brand, M. Rombach, J. Seebacher, H. Vahrenkamp, *Inorg. Chem.* **2001**, *40*, 6151–6157.
[24] M. Ji, B. Benkmil, H. Vahrenkamp, *Inorg. Chem.* **2005**, *44*, 3518–3523.
[25] M. M. Ibrahim, G. He, J. Seebacher, B. Benkmil, H. Vahrenkamp, *Eur. J. Inorg. Chem.* **2005**, 4070–4077.
[26] M. M. Ibrahim, J. Seebacher, G. Steinfeld, H. Vahrenkamp, *Inorg. Chem.* **2005**, *44*, 8531–8538.
[27] F. Fabrizi de Biani, F. Jäkle, M. Spiegler, M. Wagner, P. Zanello, *Inorg. Chem.* **1997**, *36*, 2103–2111.
[28] S. L. Guo, F. Peters, F. Fabrizi de Biani, J. W. Bats, E. Herdtweck, P. Zanello, M. Wagner, *Inorg. Chem.* **2001**, *40*, 4928–4936.
[29] A. Haghiri Ilkhechi, M. Scheibitz, M. Bolte, H.-W. Lerner, M. Wagner, *Polyhedron* **2004**, *23*, 2597–2604.
[30] A. Haghiri Ilkhechi, M. Bolte, H.-W. Lerner, M. Wagner, *J. Organomet. Chem.* **2005**, *690*, 1971–1977.
[31] A. Haghiri Ilkhechi, J. M. Mercero, I. Silanes, M. Bolte, M. Scheibitz, H.-W. Lerner, J. M. Ugalde, M. Wagner, *J. Am. Chem. Soc.* **2005**, *127*, 10656–10666.
[32] F. Zhang, T. Morawitz, S. Bieller, M. Bolte, H.-W. Lerner, M. Wagner, *Dalton Trans.* **2007**, 4594–4598.
[33] S. Bieller, F. Zhang, M. Bolte, J. W. Bats, H.-W. Lerner, M. Wagner, *Organometallics* **2004**, *23*, 2107–2113.
[34] F. Zhang, M. Bolte, H.-W. Lerner, M. Wagner, *Organometallics* **2004**, *23*, 5075–5080.
[35] S. Bieller, M. Bolte, H.-W. Lerner, M. Wagner, *Inorg. Chem.* **2005**, *44*, 9489–9496.
[36] S. T. Prigge, A. S. Kolhekar, B. A. Eipper, R. E. Mains, L. M. Amzel, *Science* **1997**, *278*, 1300–1305.
[37] S. T. Prigge, B. A. Eipper, R. E. Mains, L. M. Amzel, *Science* **2004**, *304*, 864–867.
[38] *Concepts and Models in Bioinorganic Chemistry*, (Eds.: H.-B. Kraatz, N. Metzler-Nolte), Wiley-VCH, Weinheim, **2006**.
[39] S. T. Prigge, A. S. Kolhekar, B. A. Eipper, R. E. Mains, L. M. Amzel, *Nat. Struct. Biol.* **1999**, *6*, 976–983.
[40] Tripodal bis(imidazole) thioether copper complexes have been studied as mimics of the $Cu_M$ site of copper hydroxylase enzymes: a) L. Zhou, D. Powell, K. M. Nicholas, *Inorg. Chem.* **2006**, *45*, 3840–3842; b) L. Zhou, D. Powell, K. M. Nicholas, *Inorg. Chem.* **2007**, *46*, 7789–7799; Few other copper complexes have been reported that possess the relevant $(amine)_2$thioether coordination sphere: c) N. W. Aboelella, B. F. Gherman, L. M. R. Hill, J. T. York, N. Holm, V. G. Young Jr. , C. J. Cramer, W. B. Tolman, *J. Am. Chem. Soc.* **2006**, *128*, 3445–3458; d) Y. Lee, D.-H. Lee, A. A. Narducci Sarjeant, L. N. Zakharov, A. L. Rheingold, K. D. Karlin, *Inorg. Chem.* **2006**, *45*, 10098–10107.
[41] K. Fujita, A. L. Rheingold, C. G. Riordan, *Dalton Trans.* **2003**, 2004–2008.
[42] W. Haubold, J. Herdtle, W. Gollinger, W. Einholz, *J. Organomet. Chem.* **1986**, *315*, 1–8.
[43] K. Ruth, R. E. Dinnebier, S. W. Tönnes, E. Alig, I. Sänger, H.-W. Lerner, M. Wagner, *Chem. Commun.* **2005**, 3442–3444.
[44] D. Kaufmann, *Chem. Ber.* **1987**, *120*, 901–905.
[45] M. C. Haberecht, J. B. Heilmann, A. Haghiri, M. Bolte, J. W. Bats, H.-W. Lerner, M. C. Holthausen, M. Wagner, *Z. Anorg. Allg. Chem.* **2004**, *630*, 904–913.
[46] H. Nöth, B. Wrackmeyer, *Nuclear Magnetic Resonance Spectroscopy of Boron Compounds, in NMR Basic Principles and Progress* (Eds.: P. Diehl, E. Fluck, R. Kosfeld), Springer, Berlin, **1978**.
[47] S. Bieller, M. Bolte, H.-W. Lerner, M. Wagner, *Z. Anorg. Allg. Chem.* **2006**, *632*, 319–324.
[48] H. Nöth, D. Sedlak, *Chem. Ber.* **1983**, *116*, 1479–1486.
[49] R. Amstutz, T. Laube, W. B. Schweizer, D. Seebach, J. D. Dunitz, *Helv. Chim. Acta* **1984**, *67*, 224–236.
[50] F. Becke, F. W. Heinemann, D. Steinborn, *Organometallics* **1997**, *16*, 2736–2739.
[51] a) W. Kaim, B. Schwederski, *Bioinorganic Chemistry: Inorganic Elements in the Chemistry of Life*, Wiley, Chichester, **1994**; b) J. J. R. Fraústo da Silva, R. J. P. Williams, *The biological chemistry of the elements: The inorganic chemistry of life*, 2nd ed., Oxford University Press, Oxford, **2001**.
[52] E. I. Solomon, R. K. Szilagyi, S. D. George, L. Basumallick, *Chem. Rev.* **2004**, *104*, 419–458.
[53] D. B. Rorabacher, *Chem. Rev.* **2004**, *104*, 651–697.
[54] J. M. Guss, H. D. Bartunik, H. C. Freeman, *Acta Cryst.* **1992**, *B48*, 790–811.
[55] J. W. L. Martin, G. J. Organ, K. P. Wainwright, K. D. V. Weerasuria, A. C. Willis, S. B. Wild, *Inorg. Chem.* **1987**, *26*, 2963–2968.
[56] M. K. Taylor, D. E. Stevenson, L. E. A. Berlouis, A. R. Kennedy, J. Reglinski, *J. Inorg. Biochem.* **2006**, *100*, 250–259.
[57] For five-coordinate complexes, the parameter $\tau=(\theta-\phi)/60°$ provides a quantitative measure of whether the ligand sphere more closely approaches a square-pyramidal ($\tau=0$) or a trigonal-bipyramidal geometry ($\tau=1$; $\theta$, $\phi$ are the two largest bond angles and $\theta\geq\phi$), cf. A. W. Addison, T. N. Rao, J. Reedijk, J. van Rijn, G. C. Verschoor, *J. Chem. Soc. Dalton Trans.* **1984**, 1349–1356.
[58] R. Balamurugan, M. Palaniandavar, H. Stoeckli-Evans, M. Neuburger, *Inorg. Chim. Acta* **2006**, *359*, 1103–1113.
[59] M. B. Ferrari, A. B. Corradi, G. G. Fava, C. G. Palmieri, M. Nardelli, C. Pelizzi, *Acta Cryst.* **1973**, *B29*, 1808–1814.
[60] M. Vaidyanathan, R. Balamurugan, U. Sivagnanam, M. Palaniandavar, *J. Chem. Soc. Dalton Trans.* **2001**, 3498–3506.
[61] M. Arca, A. J. Blake, V. Lippolis, D. R. Montesu, J. McMaster, L. Tei, M. Schröder, *Eur. J. Inorg. Chem.* **2003**, 1232–1241.
[62] F. Meyer, A. Jacobi, L. Zsolnai, *Chem. Ber.* **1997**, *130*, 1441–1447.
[63] For structurally characterized examples of related transition metal complexes bearing scorpionate ligands $[R(R')B(O)pz]^{2-}$ see: a) A. Carvalho, Â. Domingos, P. Gaspar, N. Marques, A. Pires de Matos, I. Santos, *Polyhedron* **1992**, *11*, 1481–1488; b) M. P. C. Campello, M. J. Calhorda, Â. Domingos, A. Galvão, J. P. Leal, A. Pires de Matos, I. Santos, *J. Organomet. Chem.* **1997**, *538*, 223–239; c) D.-L. Deng, Y.-H. Zhang, C.-Y. Dai, H. Zeng, C.-Q. Ye, R. Hage, *Inorg. Chim. Acta* **2000**, *310*, 51–55; d) Â. Domingos, M. R. J. Elsegood, A. C. Hillier, G. Lin, S. Y. Liu, I. Lopes, N. Marques, G. H. Maunder, R. McDonald, A. Sella, J. W. Steed, J. Takats, *Inorg. Chem.* **2002**, *41*, 6761–6768.
[64] S. Bieller, A. Haghiri, M. Bolte, J. W. Bats, M. Wagner, H.-W. Lerner, *Inorg. Chim. Acta* **2006**, *359*, 1559–1572.
[65] M. Albrecht, K. Hübler, S. Zalis, W. Kaim, *Inorg. Chem.* **2000**, *39*, 4731–4734.
[66] L. H. Gade, *Koordinationschemie*, Wiley-VCH, Weinheim, **1998**.
[67] W. Koch, M. C. Holthausen, *A Chemist's Guide to Density Functional Theory*, Wiley-VCH, Weinheim, **2001**.
[68] K. Kunz, H. Vitze, M. Bolte, H.-W. Lerner, M. Wagner, *Organometallics* **2007**, *26*, 4663–4672.
[69] A. J. Bard, L. R. Faulkner, *Electrochemical Methods. Fundamentals and Applications*, 2nd ed., Wiley, New York, **2001**.
[70] B. L. Vallee, R. J. P. Williams, *PNAS* **1968**, *59*, 498–505.
[71] M. C. Holthausen in *The Encyclopedia of Mass Spectrometry, Volume 1: Theory and Ion Chemistry* (Ed.: P. B. Armentrout), Elsevier Science, Amsterdam, **2003**, pp. 77–89.
[72] M. Scheibitz, M. Bolte, J. W. Bats, H.-W. Lerner, I. Nowik, R. H. Herber, A. Krapp, M. Lein, M. C. Holthausen, M. Wagner, *Chem. Eur. J.* **2005**, *11*, 584–603.
[73] P. Spuhler, M. C. Holthausen, *Angew. Chem.* **2003**, *115*, 6143–6147; *Angew. Chem. Int. Ed.* **2003**, *42*, 5961–5965.
[74] D. Schröder, M. C. Holthausen, H. Schwarz, *Organometallics* **2004**, *108*, 14407–14416.
[75] M. Schatz, V. Raab, S. P. Foxon, G. Brehm, S. Schneider, M. Reiher, M. C. Holthausen, J. Sundermeyer, S. Schindler, *Angew. Chem.* **2004**, *116*, 4460–4464; *Angew. Chem. Int. Ed.* **2004**, *43*, 4360–4363.

  

[76] C. Würtele, E. Gaoutchenova, K. Harms, M. C. Holthausen, J. Sundermeyer, S. Schindler, *Angew. Chem.* **2006**, *118*, 3951–3954; *Angew. Chem. Int. Ed.* **2006**, *45*, 3867–3869.
[77] D. Maiti, D.-H. Lee, K. Gaoutchenova, C. Würtele, M. C. Holthausen, A. A. N. Sarjeant, J. Sundermeyer, S. Schindler, K. D. Karlin, *Angew. Chem.* **2008**, *120*, 88–91; *Angew. Chem. Int. Ed.* **2008**, *47*, 82–85.
[78] A. L. Spek, *J. Appl. Crystallogr.* **2003**, *36*, 7–13.
[79] G. M. Sheldrick, *Acta Cryst.* **1990**, *A46*, 467–473.
[80] G. M. Sheldrick, *SHELXL-97. A Program for the Refinement of Crystal Structures*, Universität Göttingen, Göttingen (Germany), **1997**.
[81] R. Ahlrichs, M. Bär, H. P. Baron, R. Bauernschmitt, S. Böcker, M. Ehring, K. Eichkorn, S. Elliott, F. Furche, F. Haase, M. Häser, C. Hättig, H. Horn, C. Huber, U. Huniar, M. Kattanek, A. Köhn, C. Kölmel, M. Kollwitz, K. May, C. Ochsenfeld, H. Öhm, A. Schäfer, U. Schneider, O. Treutler, K. Tsereteli, B. Unterreiner, M. v. Arnim, F. Weigend, P. Weis, H. Weiss, *Turbomole V. 5.9 - program system for ab initio electronic structure calculations*, **2007**.
[82] J. B. Perdew, *Phys. Rev. B* **1986**, *33*, 8822–8824.
[83] A. D. Becke, *Phys. Rev. A* **1988**, *38*, 3098–3100.
[84] A. Schäfer, C. Huber, R. Ahlrichs, *J. Chem. Phys.* **1994**, *100*, 5829–5835.
[85] M. Dolg, U. Wedig, H. Stoll, H. Preuss, *J. Chem. Phys.* **1987**, *86*, 866–872.
[86] K. Eichkorn, O. Treutler, H. Öhm, M. Häser, R. Ahlrichs, *Chem. Phys. Lett.* **1995**, *240*, 283–289.
[87] R. A. Kendall, H. A. Früchtl, *Theor. Chem. Acc.* **1997**, *97*, 158–163.
[88] B. I. Dunlap, *J. Mol. Struct.* **2000**, *529*, 37–40.
[89] B. I. Dunlap, *J. Chem. Phys.* **1983**, *78*, 3140–3142.
[90] K. Eichkorn, F. Weigend, O. Treutler, R. Ahlrichs, *Theor. Chim. Acta* **1997**, *97*, 119–124.
[91] A. Klamt, G. Schüürmann, *J. Chem. Soc. Perkin Trans. 2* **1993**, 799–805.

Received: March 31, 2008
Published online: June 20, 2008

  